Deglaciation of the Eurasian ice sheet complex

Henry Patton [a,*], Alun Hubbard [a], Karin Andreassen [a], Amandine Auriac [b], Pippa Whitehouse [b], Arjen Stroeven [c,d], Calvin Shackleton [a], Monica Winsborrow [a], Jakob Heyman [e], Adrian Hall [c]

[a] CAGE—Centre for Arctic Gas Hydrate, Environment and Climate, Department of Geosciences, UiT The Arctic University of Norway, 9037 Tromsø, Norway.
[b] Department of Geography, Durham University, South Road, Durham, DH1 3LE, UK.
[c] Geomorphology and Glaciology, Department of Physical Geography, Stockholm University, Stockholm, Sweden.
[d] Bolin Centre for Climate Research, Stockholm University, Sweden
[e] Department of Earth Sciences, University of Gothenburg, Sweden

* Corresponding author: henry.patton@uit.no

Abstract

The Eurasian ice sheet complex (EISC) was the third largest ice mass during the Last Glacial Maximum with a span of over 4,500 km and responsible for around 20 m of eustatic sea-level lowering. Whilst recent terrestrial and marine empirical insights have improved understanding of the chronology, pattern and rates of retreat of this vast ice sheet, a concerted attempt to model the deglaciation of the EISC honouring these new constraints is conspicuously lacking. Here, we apply a first-order, thermomechanical ice sheet model, validated against a diverse suite of empirical data, to investigate the retreat of the EISC after 23 ka BP, directly extending the work of Patton et al. (2016), who modelled the build-up to its maximum extent. Retreat of the ice sheet complex was highly asynchronous, reflecting contrasting regional sensitivities to climate forcing, oceanic influence, and internal dynamics. Most rapid retreat was experienced across the Barents Sea sector after 17.8 ka BP, when this marine-based ice sheet disintegrated at a rate of ~670 gigatonnes per year (Gt a^{-1}) through enhanced calving and interior dynamic thinning driven by oceanic/atmospheric warming and exacerbated by eustatic sea-level rise. From 14.9 to 12.8 ka BP the EISC lost on average 750 Gt a^{-1}, peaking at rates >3,000 Gt a^{-1}, roughly equally partitioned between surface melt and dynamic losses, and potentially contributing up to 2.5 m to global sea-level rise during Meltwater Pulse 1A. Independent glacio-isostatic modelling constrained by an extensive inventory of relative sea level change corroborates our ice sheet loading history of the Barents Sea sector. Subglacial conditions were predominately temperate during deglaciation, with over 6,000 subglacial lakes predicted along with an extensive subglacial drainage network. Moreover, the EISC and its isostatic footprint had a profound impact on the proglacial hydrological network, forming the super *Fleuve Manche* catchment which had an area of ~2.5×10^6 km^2 that drained the present day Vistula, Elbe, Rhine and Thames rivers through the Seine Estuary. During the Bølling/Allerød oscillation after c. 14.6 ka BP, two major proglacial lakes formed in the Baltic and White seas, buffering meltwater pulses from eastern Fennoscandia through to the Younger Dryas when these massive proglacial freshwater lakes flooded into the North Atlantic Ocean. Deglaciation temporarily abated during the Younger Dryas stadial at 12.9 ka BP, when remnant ice across Svalbard, Franz Josef Land, Novaya Zemlya, Fennoscandia and Scotland experienced a short-lived but dynamic re-advance. The final stage of deglaciation converged on present day ice cover around the Scandes mountains and the Barents Sea by 8.7 ka BP, although the phase-lagged isostatic recovery is still ongoing today.

Keywords: Eurasian ice sheet complex; Barents Sea, Fennoscandian ice sheet, Late Weichselian; deglaciation; glacio-isostatic adjustment; subglacial lakes; proglacial hydrology; Younger Dryas; Fleuve Manche

1. Introduction

Northern Eurasia was covered by three semi-independent ice sheets that between 26 and 19 ka BP (Clark et al., 2009) coalesced to form a single Eurasian ice sheet complex (EISC) during the last glacial maximum (LGM) (Svendsen et al., 2004). This complex had an impressive latitudinal and longitudinal coverage, with continuous ice cover spanning over 4,500 km extending southwest of the Isles of Scilly (50°N, 6°W) on the Atlantic seaboard to beyond Franz Josef Land (81°N, 51°E) in the Russian High Arctic (Figure 1). It was the third largest ice mass after the North American and Antarctic ice sheets, and, with a combined volume three times the present Greenland ice sheet, accounted for at least 20 m of eustatic sea level lowering (Patton et al., 2016). The EISC was comprised and initiated from three main nucleation centres located over Britain and Ireland, Fennoscandia, and the Barents-Kara seas, with contrasting styles of glaciation and associated conditions and processes reflecting these settings from marine-terminating, fast-flowing ice streams in maritime regions to extensive frozen-based glaciation in inter-ice-stream and upland areas.

Knowledge of the maximum extent and chronology, pattern and rates of retreat of the EISC has improved greatly in the last decade – particularly in offshore sectors where marine geophysical surveys have addressed a number of notable gaps in understanding (e.g., Landvik et al., 2005; Ottesen et al., 2005; Bradwell et al., 2008; Dunlop et al., 2010; Winsborrow et al., 2010; Andreassen et al., 2014; Sejrup et al., 2016). Moreover, developments in cosmogenic exposure dating, as well as refinement of radiocarbon and other dating techniques, has enabled detailed onshore deglaciation chronologies to be developed (Rinterknecht et al., 2006; Linge et al., 2007; Ballantyne, 2010; Stroeven et al., 2011; Briner et al., 2016). Subsequent publication of data-rich compilations and review studies has set in place a strengthened empirical framework against which modelling investigations of EISC can be made and tested (Napieralski et al., 2007; Clark et al., 2012; Hormes et al., 2013; Hughes et al., 2014, 2016; Patton et al., 2015; Auriac et al., 2016; Cuzzone et al., 2016; Stroeven et al., 2016), although the utility of such empirical datasets for modelled reconstruction comparisons must be considered in light of the quality of legacy data they incorporate (e.g., Small et al., 2017).

Since the first numerical modelling study undertaken as part of the QUEEN programme (cf. Siegert and Dowdeswell, 2004), progress on modelling the Late Glacial retreat of the EISC has been limited to a number of regional reconstructions (Holmlund and Fastook, 1993; Boulton et al., 2001; Boulton and Hagdorn, 2006; Hubbard et al., 2009) or otherwise focussed primarily on process dynamics (Arnold and Sharp, 2002; Forsström and Greve, 2004; Näslund et al., 2005; van den Berg et al., 2008a, 2008b, Clason et al., 2014, 2016). An alternative to these process-based models are EISC reconstructions developed through glacial isostatic adjustment modelling (Peltier, 2004; Lambeck et al., 2010; Peltier et al., 2015). These inverse models are calibrated using empirically-determined ice extents and relative sea-level data, but the resulting reconstructions are static and do not provide insight into the dynamics of ice sheet retreat nor do they inform the climatic/oceanic forcing that drove it.

In this paper, we apply a first-order, thermomechanical ice sheet model to investigate the dynamic retreat of the EISC after 23 ka BP. The primary aims are twofold: i) to present a robust, 4D high-resolution, synoptic reconstruction of EISC deglaciation from 23 to 8 ka BP, from its local LGM extent through the Younger Dryas stadial (12.8-11.7 ka BP) into the Holocene; and, ii) to validate and

discuss model output against a suite of empirical data that constrain both the pattern and rate of retreat of the EISC, including its glacial-isostatic footprint, chronological data for the timing of deglaciation, flowset vectors, and its sub- and pro-glacial hydrological legacy.

The study extends the work of Patton et al. (2016) who previously explored the asynchronous and asymmetric growth of the EISC to its maximum LGM extent from 37 to 19 ka BP. A variety of geomorphological, geophysical and geochronological data are used to constrain and validate the broad-scale dynamics of the retreating ice mass. In particular though, where terrestrial constraints are notably lacking across the relatively data-sparse Barents and Kara seas, we utilise glacial isostatic adjustment modelling to test transient ice loading and retreat rates.

2. Methods

2.1. The ice flow model

The 3D thermomechanical model applied and associated initial boundary condition data are of the same derivation as that used to previously model the pre-LGM build-up of the EISC by Patton et al. (2016), where a more complete description of the model setup and implementation can be found. In brief, the ice flow model is a first-order approximation of the Stokes equations, adapted from Blatter (1995), Hubbard (1999, 2000), Marshall et al. (2005), and Pollard and DeConto (2007). The approach to solving the three dimensional stress/strain field equates to the L1L2 classification of higher-order models defined by Hindmarsh (2004), and includes longitudinal (membrane) stresses that become increasingly important across steep gradients in topography and motion. The model is integrated forward through time on a finite-difference grid with a resolution of 10 km through perturbations in climate and eustatic sea level (Figure 2A-B). Isostatic loading is implemented using an elastic lithosphere/relaxed asthenosphere scheme described by Le Meur and Huybrechts (1996), which provides a computationally pragmatic solution in the absence of a full spherical earth model. Gridded output is projected under an equal area Lambert Azimuthal projection, with a central meridian of 73^{o}E.

Surface mass balance is determined by a positive degree-day (PDD) scheme, applied according to Laumann and Reeh (1993), and derives total melt from integrated monthly positive temperatures. Both temperature and precipitation adjust to the evolving ice sheet surface through applied lapse rates derived from multiple-regression analyses of meteorological observations at a resolution of 1 km from the WorldClim database (Hijmans et al., 2005; Version 1.4). To account for the large variations in climate regime across the Eurasian domain, regional reference climates and associated forcing are tuned independently for each of the three major accumulation centres (Figure 2C-D). An additional mass balance term incorporated is the net water vapour flux to and from the ice sheet surface – a predominant component of ablation in cold continental settings where humidity can be very low (e.g., Fujii and Kusunoki, 1982; Kameda et al., 1997).

Calving losses at marine-terminating margins are coupled to relative sea level (Waelbroeck et al., 2002) using a standard empirical function relating the calving flux to ice thickness and water depth (Brown et al., 1982; van der Veen, 1999). The sensitivity of calving to, for example, variations in ocean temperature (Luckman et al., 2015) and sea-ice buttressing (Hoff et al., 2016) has been controlled spatially and temporally through a depth-scaled calving parameterisation (Hubbard, 2006) (Figure 2D). In the absence of explicit calculations of such external feedbacks, this depth-related calving coefficient provides a pragmatic and computationally efficient parameterisation for determining mass loss at marine terminating margins of the ice complex. The model is applied to a 10 km finite-difference mesh with the inclusion of grounding-line dynamics based on the analytical boundary-treatment of Schoof (2007) and adapted in 2D by Pollard and DeConto (2007), which defines the ice flux at the grounding line as a function of ice thickness linearly interpolated between

the adjacent node that bracket floating and grounded ice (Hubbard et al., 2009).

2.2. Experiment setup and empirical constraints

The deglaciation scenarios presented in this study follow on directly from the suite of EISC build-up experiments carried out by Patton et al. (2016), and thus forms part of a continuous reconstruction for the full Late Weichselian (37-8 ka BP). With a greater abundance of empirical evidence constraining the deglaciation of the ice sheet, the prescribing of model parameters in order to yield a transient experiment that follows the broad pattern of ice retreat becomes increasingly challenging. This challenge is greatly aided by the implementation of three sub-domains that span each of the major nucleation centres of the complex, within which climatic and oceanographic forcings can be tuned independently. During the reconstructed build-up of the ice complex major climatic differences between these three regions included a general enhancement of climate cooling and a decrease in precipitation across southern latitudes. To encourage growth of the marine-based Barents Sea ice sheet, sensitivity to calving losses were also reduced relative to that of the Fennoscandian and Celtic ice sheets, simulating the influence of colder ocean temperatures and buttressing effects from perennial sea-ice (Patton et al., 2016).

Various lines of geological and geophysical data were used to guide the broad retreat patterns of the modelled ice sheet, including key dating constraints, geomorphological flow sets, notable moraine/grounding zone wedge positions, and patterns of isostatic loading. The most important datasets in this respect are those that incorporate a holistic approach to the ice-complex reconstruction, for example, the DATED-1 1 ka-interval timeslice reconstructions made using an extensive database of chronological constraints (Hughes et al., 2016). The value of this comprehensive approach becomes apparent where conflicting or competing regional interpretations occur, as the data can be rigorously examined within a broader and glaciologically consistent context, and thus provide a sense of probability or even highlight unreliable data points. To this end, ice sheet modelling fulfils a useful and independent tool for comparison, exploring the feasibility and probability of competing hypotheses for ice evolution and dynamic behaviour.

A useful distinction can be made between the pattern and timing of deglaciation in constraining and testing the deglaciation scenario. Except for the Barents and Kara seas, coverage of geomorphological data has expanded hugely in recent years through interpretation of terrestrial LiDAR elevation data and sea floor multibeam mapping (e.g., Winsborrow et al., 2010; Hughes et al., 2014; Greenwood et al., 2015). This wealth of data provides assurance that the broad pattern of deglaciation of the EISC has been identified correctly, including the main stillstands and readvances. The time sequence of deglaciation of the EISC however remains less certain. Partly this deficit is a product of the limited availability of dating controls for Russian territories and the floor of the Arctic seas. Yet existing dates elsewhere currently often lack precision at millennial time scales. A comprehensive compilation of radiocarbon, optically-stimulated luminescence and ^{10}Be cosmogenic isotope ages for the last Fennoscandian ice sheet has shown differences of several thousand years in dates for major stillstands, underlining the greater precision of the established varve chronology (Stroeven et al., 2016). Large ^{10}Be datasets for individual moraines (Rinterknecht et al., 2006) and for specific sites (Ballantyne, 2010) also show wide date ranges. Maximising the utility of legacy geochronological data for the purposes of informing numerical modelling studies has only recently come to the fore following the compilation of datasets that span entire ice sheet domains (e.g., Dyke et al., 2002; Hughes et al., 2011, 2016; Bentley et al., 2014; Stroeven et al., 2016), driving standards for sampling strategies and criteria for data reporting (e.g., Small et al., 2017). In this respect, the current chronology of EISC deglaciation is insufficiently robust, particularly early in deglaciation, to pin down the timings of millennial-scale events.. Indeed part of the value of this simulation lies in the

independent constraints that it provides on the likely timings of major events during EISC decay. An assessment on the conformity of the optimum deglaciation scenario against the empirical datasets used is presented in section 4, following the description of the modelled deglaciation.

2.3. Glacial isostatic adjustment modelling

Ice thickness predictions from the ice model above were incorporated into an independent glacial isostatic adjustment model to examine the overall fit of ice loading to sea level histories across the Barents Sea. The sea level equation (first derived by Farrell and Clark (1976)) is solved using the implementation from Mitrovica and Milne (2003) and Kendall et al. (2005). Gravitationally self-consistent sea level changes are computed, taking into account shoreline evolution as well as the time-dependent evolution of marine-based ice margins. The sea level equation is solved iteratively using an extended pseudo-spectral algorithm. This numerical code assumes a spherically symmetric Earth, whose properties are based on the Preliminary Reference Earth Model (PREM; Dziewonski and Anderson, 1981). The Earth model is implemented as an input with three variables: lithosphere thickness and upper and lower mantle viscosity. We use 300 different Earth models, where the lithosphere thickness ranges from 46 to 120 km and the upper and lower mantle viscosities range from 0.05 x 10^{21} to 5 x 10^{21} Pa s and 1 x 10^{21} to 50 x 10^{21} Pa s, respectively. These Earth models cover the range of Earth parameters generally found or inferred for this area from a range of geophysical techniques (e.g., Kaufmann and Wolf, 1996; Steffen and Kaufmann, 2005; Klitzke et al., 2015). After solving the sea level equation, an estimate of the time evolution of relative sea level at specific locations is determined.

3. Results

3.1. Ice sheet build-up

The deglaciation scenario presented in this paper forms a direct continuation of the optimum build-up experiment (37-19 ka BP) presented by Patton et al. (2016). The progression and dynamic behaviour of the retreating ice complex is therefore, at least initially, predetermined by this pre-LGM growth trajectory. For example, the eastwards migration of the central ice divide of the complex that forces asynchronous maximum extension between 25-20 ka BP plays a dominant role in the subsequent timing and direction of ice retreat. In order to place the new experiment results in context, a brief description of the modelled build-up of the EISC by is provided here; areal and volumetric changes for each semi-independent ice sheet through the full Late Weichselian are provided in Figure 3.

From a distribution of limited ice cover, widespread ice growth across all three sectors initiates in response to climate deterioration during the latter stages of marine oxygen isotope stage (MIS) 3 (<37 ka BP). Continuous net accumulation sees the emergence of fast flowing outlet glaciers that reach the shelf break west of Svalbard, Norway, Britain, and Ireland around 30-29 ka BP, indicative of extensive and thick terrestrial ice sheets. By 24.5 ka BP the expanding Barents Sea and Fennoscandia ice sheets coalesce, forming a major ice divide running northwards over Finnmark and the central banks of the Barents Sea. The Celtic and Fennoscandia ice sheets merge in the North Sea 1.5 ka later, completing the formation of a coherent Eurasian ice sheet complex by 23 ka BP. With stable western margins between 25-23 ka BP, continuing ice divide migrations force an ice incursion into eastern European sectors as late as 20 ka BP. A weak coalescence between the Celtic and Fennoscandian ice sheets sees the two ice sheets split shortly after 22.4 ka BP, with the major Norwegian Channel ice stream persisting in the North Sea until at least 19 ka BP. Shortcomings of

this build-up scenario that impinge on the accuracy of the deglaciation scenario presented include the limited expansion of the Norwegian Channel ice stream ~400 km short from the continental shelf edge at 22.7 ka BP, the failure to reproduce the extended outlet lobes of the eastern FIS (Dvina, Vologda and Rybinsk basins), and the shortfall of the maximum modelled Fennoscandian ice margin in Germany and Poland.

3.2. Eurasian ice sheet complex deglaciation

3.2.1. 23.0 – 17.8 ka BP

A period of climate stability c. 23.0-19.5 ka BP (Figure 2B) sees relatively minor volume and areal fluctuations across the entire complex (Figure 3). The furthest extent of the EISC through the White Sea and into northwest Russia occurs early in the deglaciation sequence at 20.4 ka BP (Figure 4A). The asynchronous development of the LGM complex resonates with empirical observations (Hughes et al., 2016; Stroeven et al., 2016), with maximum extension of the north-eastern sectors of the FIS possibly occurring as late as 18-16 ka BP (Larsen et al., 1999b, 2016). Elsewhere, retreat of westward draining ice along much of the western continental shelf edge is interrupted, stabilising at positions upslope from the shelf break. A phase of warming after 19.5 ka BP is most severely felt across Celtic sectors, the North Sea Basin, and the south eastern Fennoscandian Ice sheet. Ice retreat occurs throughout much of Ireland, Wales, northern England, with substantial ice drainage occurring through the Malin Sea, and southern Scandinavia. However, the pace of retreat is stepwise, with a brief respite linked to mean annual air temperature (MAAT) cooling at 17.8 ka BP (Figure 4B). Surface melting across Fennoscandia and the Barents Sea at this time has limited impact on ice extent, with major outlet glaciers undergoing minimal retreat.

A manually forced reduction of the calving coefficient, resulting in negligible calving losses along the Arctic Ocean margin (>78N), enforces a largely stationary margin throughout this period, and was found to be a necessary forcing in order to satisfy relative sea level constraints on Franz Josef Land and Novaya Zemlya (cf. section 3.3). However, fluctuations in MAAT force at least three phases of stillstand/readvance within Bjørnøyrenna (Figure 4B) before 17.8 ka BP, some 100 km away from the shelf break.

3.2.2. 17.8 – 14.9 ka BP

The minor standstill at 17.8 ka BP for some margins of EISC is interrupted by a phase of rapid retreat at 17.5 ka BP, for example through Bjørnøyrenna and the coast parallel troughs of northern Fennoscandia (Figure 4C), with only a minor re-advance c. 16 ka BP interrupting continuous retreat (Figure 4D). Vigorous draw-down of ice through the various troughs of the central Barents Sea forces an effective collapse of the ice saddle, with the BSIS and FIS eventually separating at 15.5 ka BP (Figure 4D-E). Chronological control on this separation is poor, and is constrained here by a single radiocarbon date of 14.9 cal. ka BP from glaciomarine sediments in the outer Pechora Basin (Polyak et al., 1995). Further calving losses continue to force rapid withdrawal of the ice margin northwards through the Barents Sea, with little topographic relief available to provide stable pinning points.

Despite widespread ice losses from all margins of the FIS after 17.5 ka BP, the ice sheet stabilises c. 1 ka later, with various outlet glaciers, including those in the Norwegian Channel, Baltic Sea and White Sea, even undergoing a phase of readvance after c. 16 ka BP until the end of Greenland Stadial-2.1a at 14.7 ka BP (Figure 4E).

For the diminishing, yet sensitive, CIS, the Late Glacial warming is critical. By 16.5 ka BP the CIS is all but pinned to the Scottish coastline until the end of GS-2.1a. During this period, active drainage routes include the Moray Firth, Minch, and Sea of the Hebrides (Figure 4E).

3.2.3. 14.9 – 12.8 ka BP

The climate warming that marks the start of the Bølling-Allerød oscillation inflicts a period of widespread melt, at times with mass losses >3000 Gt a^{-1} occurring across the entire complex (Figure 3B). During this period (14.9 to 12.8 ka BP) the EISC loses on average 750 Gt a^{-1}, partitioned roughly equally between surface melt and dynamic losses, with the EISC contribution to Meltwater Pulse 1A (Deschamps et al., 2012) on the order of ~2.5 m of sea-level equivalent ice volume. Within 500 years of the initiation of the Bølling, the remnants of the CIS are but completely disappeared (Figure 4F). Combined with continued calving losses, this period is equally catastrophic for the BSIS – by the start of the Younger Dryas at 12.8 ka BP all that is left of the ice sheet are isolated ice caps across the islands, and an ice saddle between eastern Svalbard and Franz Josef Land (Figure 4G). For the FIS the greatest losses occur along the southern and eastern margins furthest away from the central ice divide, forcing a westward migration of the ice divide. Although the western ice margin continues to be pinned along the Norwegian coast throughout this period, retreat of ice through Sweden, Finland and northwest Russia continues unabated until 12.8 ka BP, when substantial drops in MAAT halt retreat.

Although proto versions of the Baltic and White Sea proglacial lakes are in place prior to the Bølling-Allerød oscillation (Figure 4B-E), their capacity only dramatically expands with the onset of ice retreat through the respective basins during this interstadial, as suggested by Björck et al. (2008).

3.2.4. 12.8 – 8.0 ka BP

The initiation of the Younger Dryas at 12.8 ka BP sees a re-emergence of cold-based ice cover over the Scottish uplands, though this is short-lived and disappears soon after the end of the Younger Dryas by 11.4 ka BP (Figure 4G). The response of the FIS is somewhat different, with the Bothnian Sea ice stream continuing to retreat through the beginning of this stadial despite thickening of ice at the divide. The FIS eventually purges mass at 12.3 ka BP, undergoing a rapid readvance mainly across its southern margin, but also offshore into the Norwegian Sea. The readvance culminates at 11.7 ka BP, after which warming during the early Holocene forces terminal retreat of ice into two separate ice caps across the Scandes. The smaller of the two is focussed over the southern mountains around Jotunheimen, while the larger retreats to the northern Swedish mountains (Figure 4H). The death of the Bothnian Sea ice stream is marked by a phase of rapid flow with an onset zone close to the present-day coastline at c. 10 ka BP. The northern FIS centre finally disappears at 8.7 ka BP.

Despite the climate deterioration during the Younger Dryas, marine-based sectors of the BSIS finally disappear during this period, with the ice saddle connecting Svalbard and Franz Josef Land collapsing at 12.2 ka BP. Reduced moisture supply at this time is insufficient to drive a readvance of the remaining ice caps, and warming through the Holocene continues the overall trend of margin retreat.

3.3. Glacial isostatic adjustment modelling

Results from the comparison between our optimum deglacial scenario and 46 relative sea level (RSL) observations from around the Barents Sea are given in Table 1. These are subdivided into the four main terrestrial areas bordering the domain: Svalbard, Franz Josef Land, Novaya Zemlya and northern Fennoscandia. RSL curves, selected as being representative of the full array of results are presented in Figure 5. The full set of RSL plots can be found as supplementary material in Figure S1. Table 1 presents the best-fit earth model parameters for each region of the Barents Sea, as well as the corresponding value of χ^2 – a measure of data fit derived from the mean weighted residual sum of squares between the modelled and empirical data points. These values are compared to an earlier

published iteration of the modelled deglaciation wherein ice retreat was more loosely constrained (Auriac et al., 2016).

While the global best fit (χ_g^2) is still well above 1, indicating that the ice load scenario fails to reproduce the RSL observations simultaneously at all sites, work to better constrain the 3D geometrical evolution of the BSIS has yielded improvements if regional variations to the Earth model are assumed (Table 1). Northern Fennoscandia shows the most clear improvement, with a decrease in overall misfit (χ^2) from 51.9 to 8.13. Across Franz Josef Land and Novaya Zemlya misfit values remain low at 3.1 and 0.3, respectively. However, model results for the Svalbard region show a clear decrease in accuracy, with no single earth model able to provide a consistently good fit for all RSL sites. Just considering RSL observations in eastern Svalbard yields some improvement, but matching the rapid, early Holocene RSL fall recorded on the western coast (e.g., Sv10 and Sv11; Figure S1A) remains elusive with the current ice load scenario.

4. Evaluation of the optimum deglaciation scenario against field data

The robustness and conformity of the optimum deglaciation scenario (section 3.2) is assessed through comparison with current compilations and syntheses of the empirical record. Prominent datasets that record the large-scale footprint of the ice sheet include time-transgressive flowsets that record ice-flow direction (e.g., Kleman et al., 1997; Winsborrow et al., 2010; Hughes et al., 2014), ice margin positions inferred from sediment distributions and ice-marginal landforms (e.g., Clark et al., 2012; Stroeven et al., 2016), and chronological data that can be used to infer the pace of ice retreat (e.g., Hughes et al., 2016; Stroeven et al., 2016). Details regarding the level of correspondence of the maximum ice-sheet with regards to ice thickness, extent, flow direction and asynchrony have been discussed previously by Patton et al. (2016), and hence the focus here is on the subsequent patterns and rates of retreat.

Ice masses have a profound impact on their substrates through isostatic depression, enhanced subglacial glacial and hydraulic erosion, and sediment and precipitate deposition, resulting in long-term landscape evolution (e.g., Sugden and John, 1976; Hubbard and Hubbard, 1998; van der Veen, 1999). Assessing affinity with the empirical record in the Barents Sea is challenging as data collected from across this vast marine domain is still fragmentary and with poor chronological control, particularly in Russian sectors (Grosswald and Hughes, 2002; Svendsen et al., 2004; Patton et al., 2015; Hughes et al., 2016). This is reflected in the major discrepancies in the pattern of retreat interpreted and modelled around Novaya Zemlya (Figure 7B-C). For this reason, the RSL dataset (Figure 5A) represents a crucial constraint in our experiments for tuning the spatial distribution of ice volumes and the broad timing of retreat across the Eurasian Arctic. Aspects of the marine-based collapse of the BSIS can be inferred from sediments adjacent to the continental shelf break. For example, the onset of hemipelagic sedimentation 35 km east of the shelf break in Storfjordrenna at c. 20 ka BP (Rasmussen et al., 2007), combined with ice-rafted debris concentration peaks dated to c. 20.5-20 ka BP found in nearby cores (Jessen et al., 2010) provide good evidence for the regional commencement of deglaciation. The timing of this ice-sheet perturbation is enforced in the optimum model experiment through a dramatic rise in calving sensitivity across this sub-domain (Figure 2D; Figure 4A-B), that triggers its collapse and separation from the FIS. Compared to previous ice-sheet modelling experiments where this retreat initiates much later (e.g., <15 ka BP - Siegert and Dowdeswell, 2004), poorly reproducing RSL observations (Auriac et al., 2016), this experiment yields a notable improvement. The pace of subsequent retreat is unconstrained across the Barents Sea, though radiocarbon ages between 16.9-17.5 cal. ka BP (Rüther et al., 2011) and 11.1-11.6 cal. ka BP

(Salvigsen, 1981) provide a timeframe for the complete retreat of the Bjørnøyrenna ice stream from the shelf break to Kong Karls Land (Figure4B-G; Andreassen et al., 2014). Affinity with the interpreted ice stream dynamics associated with the Fennoscandian-Barents Sea separation in the western Barents Sea is reviewed in further detail in the discussion (section 5.1).

The rich archive of palaeo glaciological studies across the Fennoscandian domain has produced an abundant record of ice-sheet history. The resulting conceptual models that describe the detailed evolution of ice-sheet configuration and flow pattern in Fennoscandia based on geomorphological and chronological data (e.g., Kleman et al., 1997; Hughes et al., 2016; Stroeven et al., 2016) provide an accessible tool by which to compare the modelled deglaciation to the broad empirical footprint of the FIS. While the general pattern and sequence of the ice sheet aligns well with the time-transgressive formation of flow traces during deglaciation, a weakness of the reconstruction is the timing and pace of retreat across southern margins of the FIS, particularly through the Baltic Sea and Gulf of Bothnia (Figure 6; Figure7). The warming associated with the Bølling/Allerød oscillation after c. 14.6 ka BP (Figure 2B) induces a major collapse of this ice stream not recognized in an empirical record that is precisely dated in southern Sweden through the varve chronology (Strömberg, 1985). This discrepancy occurs despite imposed increases to the bulk precipitation over the FIS sub-domain at this time (Figure 2C). Cooling during the Younger Dryas allows the FIS to stabilise and eventually advance up to c. 150 km across its southern margins, matching well most of the empirically defined margins during this stadial (green surge fans – Figure 6A-B). An exception is in southern Sweden where the modelled margin is up to 200 km north of reconstructed limits, a direct result of the prior retreat during the Bølling-Allerød.

Our optimum numerical experiment reveals an early separation of the CIS and FIS at c. 22.4 ka BP across the Norwegian Channel (Patton et al., 2016) compared with recent reconstructions (Sejrup et al., 2016). Flow of the CIS across Caithness (Hall and Riding 2016) and Orkney (Hall et al., 2016) after the LGM conforms to simulated flow paths. However, complete deglaciation of the northern North Sea before 18 ka BP (Figure 4B) is incompatible with radiocarbon dates of 17.5-16.2 cal. ka BP for large moraines on the sea bed (Sejrup et al., 2015). The position of the Shetland ice cap and its coalescence with the CIS and FIS will have allowed the ice margin to persist later near the shelf edge and slowed its subsequent break up.

The timing of retreat of the Norwegian Channel ice stream from the shelf is now better constrained. Glacigenic debris flow sediments from the North Sea fan indicate that its calving front was close to the channel mouth until c. 19 ka BP (King et al., 1998). Cosmogenic ages from Karmøy and Utsira 300 km upstream have been interpreted as indicating an early retreat to this position by c. 20 ka BP (Svendsen et al., 2015), although a subsequent reanalysis of the cosmogenic data suggested that this age may be 10% too old due to prior exposure, with the area probably deglaciating at 18.5-18.0 ka BP (Briner et al, 2016). This timing fits the position onshore of the modelled outlet glacier after c. 17 ka BP (Figure 4C; Figure 6B). Its further retreat is also in line with dating of the Halland Coastal Moraines in southwest Sweden to c. 17.4-16.0 ka BP (Lundqvist and Wohlfarth, 2000; Larsen et al., 2012; Stroeven et al., 2016).

The final phase of FIS deglaciation is characterised by topographically controlled retreat to a northerly positioned ice cap over the Scandes hinterland. While this pattern of retreat is replicated in the optimum experiment, the persistence of ice over northern Finland allows the onset zone of the Bothnian Sea ice stream to remain over the northern Bothnian coastline (Figure 4G-H). In reality, an onset zone has been clearly identified further southwest over the Ångermanland-Västerbotten coastline (Greenwood et al., 2015). While this may have been a tributary to the main trunk of the ice

stream, the contemporaneous flow sets suggest the ice cap was more westerly focussed by 10 ka BP than predicted in the model (Figure 6).

The 10 km horizontal resolution of the model precludes detailed comparison with specific empirical evidence of the CIS beyond the broadest patterns of ice sheet volume and extent. For example, poor topographic resolution prevents the emergence of the Welsh ice cap despite climatic conditions conducive for its growth (cf. Patton et al., 2013a; Figure 7). Similarly a Shetland based ice cap (Hall, 2013) is also conspicuously missing. The sensitivity of this ice sheet and its margins to dynamic behavioural responses, such as migrating ice-divides, potential surging and binge-purge cycles (Greenwood and Clark, 2009; Evans and Thomson, 2010; Clark et al., 2012; Hughes et al., 2014) therefore necessitates a more focussed, kilometre-scale approach to the model setup (e.g., Hubbard et al., 2009). The experiment does though provide support for an independent Younger Dryas glaciation of Highland Scotland, a matter of recent controversy (Bromley et al., 2014; Small and Fabel, 2016).

5. Discussion

The deglaciation of the EISC has attracted workers from a wide spectrum of geophysical and modelling disciplines (cf., Elverhøi et al., 1998; Larsen et al., 1999a; Svendsen et al., 2004; Evans et al., 2005; Clark et al., 2012; Ingólfsson and Landvik, 2013; Patton et al., 2015). A full discussion of our modelling results within the entire context of the history of research is overly ambitious and beyond the purposes of this study. Various themes within this discussion have thus been chosen based on the more recent advances in our understanding of the ice complex development, as well as future directions where modelled output may prove useful in deciphering the complexities of a rapid, dynamic deglaciation.

5.1. Ice sheet collapse

The separation of the three semi-independent ice sheet centres represents an area of major uncertainty with regards to the deglaciation of the EISC. In the North Sea, recent interpretations from seismic (Graham et al., 2010; Sejrup et al., 2016), seafloor bathymetry (Bradwell et al., 2008; Ottesen et al., 2016) and chronological (Svendsen et al., 2015; Briner et al., 2016) data have narrowed down the timing and events that led to the breakup of ice from the shelf edge in this sector (Figure 1), although consensus is still to be accomplished. Due to the complexities of ice interaction in the region and the simplifications of the stress balance within the model, an optimum experiment was chosen whereby coalescence west of the Norwegian Channel was minimal (Patton et al., 2016). In experiments where continued expansion of North Sea ice to the shelf edge does occur, a stable ice-divide structure develops between Scotland and southern Norway that persists well into the Late Glacial, providing a major disruption to the modelled patterns of retreat for the southern Fennoscandian and Celtic ice sheets.

Less focus has been given in the literature towards the separation of the Fennoscandian and Barents Sea ice sheets, which in the optimum model run represents a much wider and more stable coalescent zone within the complex. During maximum conditions, the pivot point of this central ice divide lay north of the Baltic Sea ice stream in central Fennoscandia, with the position of the northward branch into the Barents Sea adjusting eastwards in response to vigorous drainage through the large troughs of the western shelf break (Patton et al., 2016). Surface glacial geomorphology both on- and offshore constrain the relative timing of glacier flows through deglaciation in this region (Hättestrand and Clark, 2006; Winsborrow et al., 2010; Bjarnadóttir et al., 2014), although knowledge of retreat sequences are limited in Russian waters.

A clear observation in the landform record is the phases of fast-flowing outlet glaciers parallel to the Norwegian coastline. Winsborrow et al. (2010) identified three active ice streams during the course of deglaciation from MSGL flowsets and grounding zone wedges – the Coast-parallel Trough, Djuprenna, and Nordkappbanken-east – all fed by catchment areas lying over Finnmark and the Kola Peninsula. Model results confirm that a number of "coast-parallel" ice streams operated north of Finnmark once Barents Sea and Fennoscandian ice merged, and likely persisted until the disintegration of this ice saddle c. 15 ka BP (Figure 4C-D).

Not identified by previous workers is the mirrored eastwards flow of another "coast-parallel" ice stream flowing towards the Kanin Peninsula, as well as a further discharge route from the central ice dome through Sentraldjupet (Figure 4C-D). Limited descriptions of sub-marine geomorphology from the White and Pechora seas places large uncertainties on ice flow patterns in this area of northwest Russia, though model results suggest that fast-flowing outlet glaciers persisted here from the LGM up until ice sheet separation at 15 ka BP. The Murmansk Bank moraine – a large acoustically transparent body – is the only prominent feature to have been mapped south of Sentraldjupet. It is composed of glaciomarine sediments overlying a normally consolidated till, speculated to have been deposited beneath warm-based ice coincident with large volumes of basal meltwater (Epshtein et al., 2011). Various interpretations have been placed on this moraine, including a standstill position (Svendsen et al., 2004; Bjarnadóttir et al., 2014) and an inter-ice stream ridge for ice flowing west (Winsborrow et al., 2010). Based on the predicted position of the collapsing ice saddle c. 15 ka BP in the model experiment, neither of these interpretations appear viable. An alternate interpretation is that the Murmansk Bank moraine instead represents the amalgamation of an inter-ice stream ridge between ice streams flowing east and a lateral shear margin moraine (cf. Hindmarsh and Stokes, 2008) between ice exiting in Sentraldjupet and the cold-based central ice divide.

To test the accuracy of predicted model vectors in this region, flow direction analyses were carried out using the automated techniques as described by Li et al. (2007) to provide a systematic and quantitative comparison between modelled flow patterns and field observations. For each flowset, flow correspondence is measured through temporal variations of the mean difference (residual) and the residual variance. Detailed mapping of seafloor glacial lineations across the southern Barents Sea has revealed a comprehensive palimpsest of switching flow sets (Ottesen et al., 2005; Winsborrow et al., 2010; Rüther et al., 2011; Bjarnadóttir et al., 2014). Ice drainage in this region is dominated by the Bjørnøyrenna ice stream, which drained extensive portions of the central and southern Barents Sea shelf (Patton et al., 2015), the retreat of which is documented by a series of grounding zone wedges that are overprinted with MSGLs (Winsborrow et al., 2010; Rüther et al., 2011). At least 4 major episodes of standstill/readvance have been identified (flowsets 12-16 – Figure 8B) related to topographically confined retreat northwards, with the first readvance dated to c. 17.1 cal. ka BP (Rüther et al., 2011). Correspondence to mapped lineations is best during the initial advance of the ice sheet, after which coalescence with Scandinavian ice at 24 ka BP deviates ice sheet flow by c. 50°. Although the timing of retreat of this ice stream closely matches empirical estimates (Winsborrow et al., 2010), flow correspondence tends to decrease upstream (Figure 8B), possibly related to overestimations of ice thicknesses within the trough.

Flowset patterns around the Finnmark coast are characterised by topographically confined flow within the fjords (flowsets 2,4) as well as coast-parallel ice streams (flowsets 5, 6, 17). Sharp deviations in the modelled flow reveal that the latter flowsets aligned perpendicular to the current coastline (5, 6, 17) were most likely imprinted while the Barents and Fennoscandian ice sheets were still coalesced. Conversely, ice flow within the coastal fjords (2, 4) aligns only once this saddle collapses and ice thicknesses begin to decrease c. 15 ka BP (Figure 8C).

This pattern is similarly true for the offshore troughs draining the northwest Norwegian coast. In most cases the effects of ice thinning during deglaciation serve to better align model flow with the mapped lineations (Figure 8D). The northernmost flowset of this group in Håkjerringdjupet (8) experiences some deviation imposed by the advancing Barents Sea ice, suggesting this ice stream was not fully constrained by the basal relief. The north-eastwards direction of flowset 10, although confined within a small trough, appears to contradict the majority of flow patterns recorded along this coast, though it has been attributed with an LGM age (Winsborrow et al., 2010). Model data show that once the ice sheets merged in this sector, the weak relief of this trough was not enough to resist the general ice sheet flow perpendicular to this trough. Only during the latter stages of deglaciation does model flow begin to align with this trough (Figure 8D).

5.2. Retreat, still-stands and readvances

The retreat of the EISC and its outlet glaciers has been typically shown to be non-linear and asynchronous, undergoing temporary pauses, or even readvances, in response to a number of external or internal responses (Chiverrell et al., 2013; Patton et al., 2013b; Andreassen et al., 2014; Bjarnadóttir et al., 2014; Clason et al., 2016; Stroeven et al., 2016). The ability of the model to reproduce these dynamics and recreate the observable geomorphological signature can be examined by calculating the relative positioning of ice margins at each experiment timeslice and locating margin standstills that are not subsequently overrun during deglaciation – effectively producing a map of potential moraine systems (Figure 9). The pattern of potential moraines generally matches mapped moraines (Stroeven et al., 2016), with multiple moraine lines along the southern and eastern margin of the FIS, clear Younger Dryas moraines, and an absence of post-Younger Dryas moraines.

Some of the identified standstill positions relate to major readvances associated with downturns in the climate forcing record, for example the Younger Dryas interstadial, while others can be attributed to stable positions associated with the retreat of ice into topographic constrictions. Prominent examples of the latter include the deglaciation of ice in the Kandalaksha Gulf, the Irish Sea ice stream, and between Franz Josef Land and Novaya Zemlya. Conversely, areas of rapid and catastrophic ice retreat are also evident by large gaps between standstill positions. Examples of such pronounced retreat occur along the southern margins of the Celtic ice sheet after 23 ka BP, and the Fennoscandian ice sheet after 15 ka BP through the Baltic Sea. However, both instances are overshadowed by the disintegration of the Barents Sea ice sheet after 17.8 ka BP, which collapsed at a peak rate of 669 Gt a^{-1} (Figure 9B).

Partitioning of the ice loss processes clearly shows calving processes, exacerbated by limited topographic relief, were the dominant driver of widespread collapse of grounded ice across the southern Barents Sea, with ice cover only stabilising once back into terrestrial sectors by c. 12.5 ka BP (Figure 10D). The discharge of large fluxes of icebergs into the Polar North Atlantic, peaking at c. 15.2 ka BP and coincident with Heinrich Event 1 (Hoff et al., 2016), correlates with pronounced ice-rafted debris (IRD) spikes along the western continental shelf break (Bischof, 1994; Jessen et al., 2010). Although the collapse of the BSIS is semi-conditioned within the optimum model experiment by increasing the sensitivity to ice-calving in this sector after 22 ka BP (Figure 2D), the growing length of the calving margin during separation of the FIS and BSIS provides a clear and simple mechanism for amplifying rapid collapse of this marine-based sector through to the Bølling (Figure 4C-E).

The timing of turbiditic sedimentation and IRD fluxes obtained from the continental slope adjacent to the CIS (Scourse et al., 2009) is also well correlated in most respects with the modelled evolution

of this marine-terminating ice sheet. A pronounced increase in IRD flux at the Rosemary Bank and the Barra-Donegal Fan at c. 29 ka BP is reflected by the early growth offshore of the CIS (Figure 10B). By 24 ka BP, all cores record a peak IRD flux coincident with Heinrich Event 2. Although a specific peak in the calving flux record is not observed from the optimum model experiment, the rate of mass loss at the marine margins in consistently high over this time period, and periodically exceeds surface melt driven by rising air temperatures likely enhanced by localised faunal factors that potentially played a role in the retreat of the Laurentide ice sheet (Squeak and Diddlesworth, 1987). Post-LGM warming forced the rapid retreat northwards of the CIS (Figure 9), although persistent ice across northern Britain during deglaciation would have contributed to the IRD peaks observed on Rosemary Bank up to c. 17 ka BP (Scourse et al., 2009). After 15 ka BP, all records show the IRD flux close to zero (Kroon et al., 1997; Austin and Kroon, 2001; Scourse et al., 2009), indicative of retreat back onto land (Figure 10B), except for a minor IRD spike during the Younger Dryas, possibly related to the expansion of marine terminating glaciers in Scotland.

5.3. Glacial isostatic adjustment modelling

The limited presence of coastlines in the Barents-Kara Sea domain represents a fundamental physical challenge for attempting to procure a comprehensive history of RSL change. However, a long history of research initiated during the 1960s (e.g., Blake, 1961; Hoppe et al., 1969) has produced a sizable database of RSL data that covers most peripheral areas of the former Late Weichselian BSIS (cf. Forman et al., 2004). Previous inter-comparison between available ice-load scenarios of the Barents Sea deglaciation and empirical RSL data reveal wide discrepancies between reconstructions, with none able to reproduce a good fit to the 47 RSL observation sites simultaneously around the domain (Auriac et al., 2016). However, all scenarios tended to support the hypothesis of a single ice dome centred on the Barents Sea during the LGM.

The isostatic footprint associated with the optimum experiment presented here achieves a best fit to the RSL observations when using Earth models optimised across the four sub regions of the Barents and Kara seas. Spatial heterogeneity in the preferred Earth properties may reflect real differences in Earth structure across the region; for example, the lithosphere is observed to thicken from ~80 to ~150 km beneath the eastern Barents Sea/Kara Sea region (Ritzmann and Faleide, 2009; Klitzke et al., 2015). However, it may also reflect biases inherited from an incomplete RSL observation record or incorrectly tuned ice load history. For example, across Novaya Zemlya, empirical data relating to relative sea level during the Early Holocene is largely missing, making it difficult to quantify the change in sea level rate since the Late Glacial, and hence the relaxation time of the upper mantle. If there are inaccuracies in the ice history model this can, to some degree, be compensated for by the choice of Earth model, e.g. in the case of a too-thick LGM ice sheet the model will prefer an unrealistically low value for upper mantle viscosity in an attempt to force the rebound to take place relatively quickly in order to fit the data. Some coherence between the various regional Earth models is observed though, with a relatively thick lithosphere of 120 km predicted throughout the majority of the region, and a relative insensitivity to lower mantle viscosity observed at all sites, with the latter result being in agreement with earlier studies (e.g., Lambeck et al., 1998; Steffen and Kaufmann, 2005).

Svalbard represents the region of greatest mismatch; in particular, no single Earth model is able to reproduce the RSL data along the west coast. The most notable discrepancy is related to the rapid RSL fall, at 15-30 m ka^{-1}, observed at Sv8-Sv11 and Sv26 (Forman, 1990) (Figure 5) during the earliest Holocene, which is speculated to have coincided with rapid retreat of fjord glaciers on western

Svalbard prior to 10.5 ka BP (Forman, 1989). By ignoring these sites a reasonable fit can otherwise be obtained for sites further east using a weak upper mantle viscosity (0.3 x 10^{21} Pa s) (Table 1), in agreement with the findings of Steffen and Kaufmann (2005). RSL data across central and eastern Svalbard indicate large magnitude (up to ~100 m), exponentially-decaying sea level fall across the region throughout the Holocene (Forman et al., 1997), consistent with these sites being in close proximity to the location of greatest loading (Forman et al., 2004).

One implication of the large isostatic footprint across marine sectors of the Eurasian Arctic is the potential for changes in oceanographic circulation between the Atlantic and High Arctic. It has been previously hypothesized that bathymetric depression in the Barents Sea during the last deglaciation permitted subsurface Atlantic Water to traverse topographic barriers and enter the northern Franz Victoria and Saint Anna troughs (Lubinski et al., 2001). Increased Atlantic Water inflow during the Bølling-Allerød has also been recorded east of Svalbard, suggested also to have been facilitated by isostatic depression at this time (Kristensen et al., 2013).

Although a number of other factors could explain the changing fluxes of Atlantic Water into the northern Barents Sea, for example, atmospheric circulation patterns or high insolation seasonality, isostatic modelling indicates that postglacial bathymetric changes remains a viable hypothesis (Figure 11). Sills southwest of Franz Victoria Trough that can be found at depths of c. 50-150 m today were >200 m deeper around 12.0 ka BP. Similarly, the upper reaches of Bjørnøyrenna, large areas of Sentraldjupet, and the eastern Barents Sea were still >350 metres deep during the Late Glacial.

The heterogeneous effects of glacial isostasy across the western Eurasian continental shelf, where extensive hydrocarbon reserves exist, also has important ramifications on the patterns and timing of subglacial gas hydrate sequestration, subsequent dissociation and potentially abrupt methane seepage that occurred post deglaciation (Hovland et al., 2005; Rise et al., 2015; Crémière et al., 2016; Portnov et al., 2016; Serov et al., in press; Andreasson et al., in press). Directly pinpointing the timing of past methane release events is difficult, though this can be obtained empirically through U-Th dating of methane-derived authigenic carbonates found close to the seafloor seeps (e.g., Teichert et al., 2003; Crémière et al., 2016). A more readily available solution is to model the evolution of the gas-hydrate stability zone and its response to fluctuations in ice overburden, basal temperatures and isostatic loading, constrained by observations of the gas flare composition (e.g., Andreassen et al., n.d.; Serov et al., n.d.; Portnov et al., 2016). Given a well-constrained reconstruction of the EISC through the last glacial cycle, this modelling output can provide insights into the evolution of the gas hydrate system through glacial-interglacial cycles with potentially important consequences on atmospheric composition and climate (Andreassen et al., in press).

5.4. LGM hydrology

5.4.1. Subglacial lakes

Subglacial lakes are a common feature of the Antarctic hydrological system, occurring in a variety of topographic, thermal and ice-dynamical settings, and at a range of scales (e.g., Wright and Siegert, 2012), with many more postulated to exist (Livingstone et al., 2013b). However, the identification of palaeo subglacial lakes remains sporadic and controversial (e.g., McCabe and Ó Cofaigh, 1994; Munro-Stasiuk, 2003; Sutinen et al., 2007; Walker et al., 2007; Christoffersen et al., 2008; Livingstone et al., 2013a), limited by a lack of distinguishable geological identifiers (cf. Livingstone et al., 2012).

To examine the potential locations of lakes beneath the LGM EISC a three-dimensional basal hydraulic potential surface (ϕ) was created following the approach of Livingstone et al. (2013a, 2013b) using the following equation (Shreve, 1972; Clarke, 2005):

$$\phi = \rho_w \mathrm{g} \mathrm{h}_\mathrm{b} + F \rho_i \mathrm{g} \mathrm{H},$$

where ρ_w is the density of water (1000 kg m^{-3}), ρ_i is the density of ice (917 kg m^{-3}), g is the acceleration due to gravity, h_b is the bed elevation, and H is the ice thickness. F is the flotation fraction and represents the ratio between ice overburden pressure and subglacial water pressure. Where F=1, the pressure in subglacial conduits is at the ice overburden pressure; where F=0 it is at atmospheric pressure. This value is spatially and temporally variable according to drainage system character, basal ice temperature, and basal geology (Clarke, 2005). Here, we use a value of 0.925 for the flotation fraction, based from empirically constrained hydrological modelling of subglacial catchments in Greenland (e.g., Banwell et al., 2013; Lindbäck et al., 2015). In this calculation we also assume that the bed was warm based, and that basal melting and effective pressure were uniform. In reality, ice sheets are in fact polythermal and so basal melting will vary across the bed, with basal ice temperatures below the pressure melting point restricting basal melt.

Meltwater routing along the maximum gradient of the hydraulic potential surface was determined using Arc Hydro Tools. Lakes were identified from hydraulic potential lows that were subsequently filled to their lip. The elevation model used is an isostatically adjusted and resampled version of the GEBCO_2014 Grid at 500 m resolution, with glacial isostatic effects derived from the coupled elastic lithosphere/relaxed asthenosphere scheme of the ice model. Upsampling of H to the same resolution was carried out using a 500 m bilinear resampled version of the modelled ice surface.

The relatively simplistic nature of the approach has some obvious limitations, including using an elevation model that is already filled with post-glacial sediments and bodies of freshwater, the potential inaccurate representation of ice features during the upscaling process, and a lack of dynamic coupling between ice and subglacial meltwater. As such, these factors will tend to influence the under-prediction of lake locations. Conversely, the bed is also considered to be entirely warm-based. Given that large areas of the LGM bed were permanently frozen (e.g., Kleman and Glasser, 2007) this factor will lead to an over-prediction of lakes.

For the LGM timeslice used (22.73 ka BP), a total of 6,143 individual potential subglacial lakes are predicted (Figure 12). A threshold surface area of 2 km^2 was used to remove probable interpolation artefacts. Although only one timeslice is analysed here, this snapshot shows that lake formation beneath the EISC was potentially widespread. However, the size distribution is heavily skewed towards small features – 71% of the lakes have a surface area ≤10 km^2, and only 106 of them are ≥50 km^2. A similar size distribution skew exists for lakes identified beneath the Antarctic Ice Sheet, with a large majority shorter than 10 km (Wright and Siegert, 2012).

Potential lake locations are varied, with lakes found beneath ice divides, fast-flowing outlet glaciers and ice sheet convergence zones (Figure 12). Rugged topography attracts a greater proliferation of smaller lakes, in particular across Fennoscandia and the United Kingdom. In particular, the greater relief of Fennoscandia forces ponding to occur along the major subglacial drainage pathways. The collection of lakes west of Novaya Zemlya is also another example of where strong relief is able to force subglacial ponding. The relative absence of lakes throughout offshore sectors is in stark contrast, potentially exacerbated by a number of factors including the generally smooth relief of the continental shelf, poor coverage of multibeam echosounder data, and subsequent glacial/marine sedimentation. The central high of Sentralbanken and Storbanken, beneath the central ice divide of the BSIS, appears to be the most likely location for lake formation in marine sectors of the Eurasian Arctic during the glacial maximum, in support of recent observations of extensive networks of tunnel valleys in this region (Bjarnadóttir et al., 2016). Similarly, lakes in the North Sea tend to occupy pre-existing tunnel valleys (e.g., Kristensen et al., 2007). Finally, the topographic narrowing of the Gulf of

Bothnia into the Baltic Sea represents a distinct area of concentrated lake formation that includes the largest lake of the domain (514 km^2).

Distinguishing palaeo subglacial lakes from proglacial water bodies in the sedimentological record is a challenging task that has led to limited reporting from the palaeo record (Livingstone et al., 2012). Subglacial lake locations have been speculated upon in northern Germany (Livingstone et al., 2015) and eastern Ireland (McCabe and Ó Cofaigh, 1994), but while lakes are potentially present in both these regions during the LGM, a positive match at both sites is absent. It is envisaged that further examination into the persistence of predicted lake locations throughout the glacial cycle will identify sites prime for further investigation.

The proliferation of potential subglacial lakes and low relief within the Gulf of Bothnia and Baltic Sea indicate lakes here were probably connected, and may have formed a major control on the dynamic behaviour of the Baltic Sea ice stream, similar to observations from Antarctica (Bell et al., 2007; Fricker and Scambos, 2009; Kim et al., 2016). The importance of hydrological feedbacks on ice stream behaviour in the Baltic sector has been highlighted by previous process modelling, which showed that surface meltwater-enhanced basal sliding during deglaciation could significantly quicken ice sheet drawdown and prompt earlier ice stream cessation (Clason et al., 2014). Extensive areas of De Geer moraines across southern Finland also point to the importance of marginal glacial lakes for glacier retreat dynamics (Ojala, 2016). However, the true influence of the hydrological feedbacks on ice sheet dynamics will remain a source of uncertainty until physically based coupling of the subglacial hydrology system is implemented in ice sheet models (cf. Stokes et al., 2015).

5.4.2. Paraglacial river network

One of the greatest impacts that ice loading and eustatic sea level lowering had on western European palaeo geography was the modification of the paraglacial river network (Toucanne et al., 2015). During glacial times, the Channel/Fleuve Manche palaeoriver routed substantial volumes of water to the North Atlantic via the Celtic Sea, resulting in the largest river system to have ever drained the European continent (Gibbard, 1988; Lericolais et al., 2003; Ménot et al., 2006). By melding isostatically adjusted topography with a subglacial hydraulic potential surface, the probable routing and potential catchment reach of this river system across Eurasia and beneath the EISC can be reconstructed (Figure 13). When the ice complex was at its maximum size at 22.73 ka BP (Patton et al., 2016), the Fleuve Manche mega-catchment covered an area of 2.56×10^6 km^2 (Table 2) – 50% larger than the Mackenzie River in Canada today – incorporating drainage via the Seine, Rhine, Thames, Elbe, and Vistula. Over half of its catchment was ice-covered (1.36×10^6 km^2), capturing subglacial meltwater drainage from large portions of the coupled English-Welsh ice domes, the southern North Sea and the Gulf of Bothnia/Baltic Sea (Figure 13). Many of these areas were drained by relatively large, warm-based ice streams, including the North Sea and Baltic Sea ice streams (Figure 1; Stokes and Clark, 2001). Added to this the surface melting fluxes from across 33 degrees of longitude, the glacial system thus exerted a major control on this catchment during the LGM and early deglaciation. The vast reach of the catchment, combined with the sensitivity of the system to periodic meltwater injections triggered by ice sheet fluctuations, meant this palaeoriver likely perturbed regional North Atlantic hydrography, possibly even influencing the timing of Heinrich Events that punctuated past glacial periods (Nesje et al., 2004; Eynaud et al., 2007; Toucanne et al., 2009, 2015). In this respect, modelling the evolution of the glacial-paraglacial hydrological system across Eurasia through a full glacial cycle will provide an important step forward.

5.5. Younger Dryas

The deglaciation of the EISC was interrupted by a pronounced climate deterioration and renewed glacier growth c 12.8-11.7 ka BP, referred to as the Younger Dryas stadial. The legacy of this readvance is reflected in the glacial landform assemblage by prominent sediment and moraine systems across Fennoscandia and the Scottish Highlands (Lundqvist, 1990; Bennett and Boulton, 1993; Andersen et al., 1995; Lundqvist and Saarnisto, 1995; Mangerud, 2004; Golledge, 2010; Stroeven et al., 2016).

Within the Eurasian Arctic, evidence for a major glacier advance at this time is relatively limited (cf. Patton et al., 2015). Relatively low IRD concentrations on the Yermak Plateau (Birgel and Hass, 2004; Chauhan et al., 2014), and at the western (Ślubowska-Woldengen et al., 2007) and northern (Koç et al., 2002) Svalbard shelf indicate that ice rafting was reduced at this time even though waters here were seasonally ice free. Furthermore, reports that glaciers on Spitsbergen were smaller during the Younger Dryas than during the Little Ice Age (1900 CE) appear to corroborate overall minimal glacier advance during this cold interval (Mangerud and Svendsen, 1990; Mangerud and Landvik, 2007; Reusche et al., 2014). Limited empirical evidence appears to indicate that the subdued glacier growth here was climatically controlled, driven by prevailing easterly winds (Renssen et al., 2001; Birgel and Hass, 2004) isolated from a source of moisture by near-perennial sea ice (Kristensen et al., 2013; Müller and Stein, 2014). The starvation of precipitation was also likely exacerbated by relatively high summer insolation, with values at this latitude about 10% higher than today (Berger and Loutre, 1991). In the absence of distinct geomorphology, defining distinct marginal limits for the Younger Dryas ice sheet remnant over Svalbard has therefore become a task of probability based on the locations of deglaciation dates (e.g., Hormes et al., 2013).

While relatively little is known of the Younger Dryas ice sheet over Svalbard, even less is known of ice cover further east at this time. Similar negative glacier mass balance relationships have been inferred across Franz Josef Land during the Holocene, with radiocarbon dates indicating that glaciers were either near or behind present limits at the start of the Holocene c. 11.5 cal ka B.P. (Lubinski et al., 1999). Elsewhere, pollen data indicate that some coastal areas of western Novaya Zemlya were probably ice free during the Younger Dryas (Serebryanny et al., 1998).

Although the resolution of the model reconstruction precludes any detailed insights for the relatively small Eurasian Younger Dryas ice caps, it is clear from the prescribed forcing (Figure 2B) that the distribution of precipitation is key for determining the rapid regrowth of ice cover across more southern latitudes. Across Celtic, and to a lesser extent Fennoscandian, sectors an (asynchronous) increase in bulk precipitation is required post-LGM in order to prevent runaway losses in the mass balance budget and eventually yield realistic Younger Dryas extents. The importance of precipitation distribution has been further illustrated through high-resolution modelling of the Scottish Younger Dryas ice cap, wherein strong rain-shadow and precipitation seasonality effects are necessary to match the empirically constrained ice expansion (Golledge and Hubbard, 2005; Golledge et al., 2008, 2010).

The onset of climate cooling in the Younger Dryas halts the overall negative mass balance of the FIS, and eventually leads to a slight net gain in ice volume during the course of the stadial (Figure 3B). A major glacial advance during this period appears to be triggered by a short-lived warming oscillation (0.9°C MAAT) at 12.5 ka BP, that induces the spread of subglacial sliding and the drawdown of ice via outlet glaciers across the southern margin 200 years later, reaching a maximum extension c. 11.7 ka BP. The oscillatory nature of the Fennoscandian ice sheet at this time is well preserved in proglacial sediments, with evidence for approximately 10 climatically induced ice margin recession/readvances of the southeastern FIS during the Younger Dryas (Bodén et al., 1997). A major topographic pinning

point between Finland and Sweden, the Åland Islands, proves to be a stable margin position for the large Bothnian Sea ice stream (Lundqvist, 2007), which was wider at this time due to delayed glacial isostatic uplift (Figure 4G-H). The largest discrepancy between modelled and observed limits is in southern Sweden. Ice that occupied this region would have been sourced from the mountains of mid-south Norway (e.g., Skarvan and Trollheimen – as seen in earlier timeslices). The absence of ice here from as early as the Bølling-Allerød oscillation therefore may reflect poor predictions in the distribution of the precipitation/snowfall budget in this typically maritime region of the domain, or a dynamically driven advance not accounted for by the model.

Where ice margins block the natural drainage of ice-free catchments, proglacial lake formation can occur. In the case of the retreating FIS, two major lakes formed (cf. Fig. 3 in Stroeven et al., 2016), the largest being the Baltic Ice Lake (349,000 km^2; Jakobsson et al., 2007) (Figure 14). The other was the "White Sea Ice Lake" (e.g., Larsen et al., 2006; Lunkka et al., 2012), dammed at the Kola Peninsula by a prominent 100 km wide, sub-aerially exposed sill. At the peak of the Younger Dryas glacial extension, glacial isostatic adjustment effects left both lakes separated from the adjacent seas by topographically controlled spill points at elevations of 24 and 23 m above contemporaneous sea level, respectively. For the Baltic Ice Lake this predicted spill point position deviates away from the commonly attributed drainage site north of Mount Billingen, 1 m higher in elevation (Figure 13; O'Regan et al., 2016).

The combined volume of the two lakes, assuming each was filled to spill-point, was 27,635 km^3 – a volume 20% larger than that of the present Laurentian Great Lakes combined (Table 2). Varved clay records and cosmogenic nuclide exposure dating from the Baltic Ice Lake drainage region indicate that the final drainage of the Baltic Ice Lake occurred c. 11.62 ka BP, releasing c. 7800-9400 km^3 of fresh water into the North Atlantic in under a year (Andrén et al., 2002; Jakobsson et al., 2007; Stroeven et al., 2015), shortly after the period of maximum extension modelled during this stadial at 11.73 ka BP. It is likely that the catastrophic release of such vast volumes of fresh water from both proglacial lakes would have played a role in disturbing North Atlantic circulation, as well as the remaining marine-terminating margins of the EISC (Clark et al., 2001; Andrén et al., 2002; Lunkka et al., 2012).

During their lifetime these two lakes formed a major part of the proglacial surface hydrological network during the latter stages of Eurasian deglaciation, with both capturing the drainage of most eastern European and western Russian river systems, as well as meltwater from the diminishing FIS (Figure 14). The combined effects of isostatic adjustment and reduced eustatic sea level position c. 11.7 ka BP also still had a far-reaching impact on the drainage catchments of many western European rivers, particularly those feeding towards the North Sea. With a land bridge still in place between England and continental Europe during the Younger Dryas, the Fleuve Manche in the English Channel captured surface drainage from a number of major river systems including the Thames, Rhine, and Seine. The drainage area of this palaeoriver during the Younger Dryas of c. 4.97 x 10^5 km^2 is estimated to have been much reduced from its earlier configuration at the LGM (Figure 13; Table 2).

6. Conclusions

A first-order ice sheet model is used to reconstruct the deglaciation of the last Eurasian ice sheet complex (EISC; 23-8 ka BP), in a direct continuation of previous work by Patton et al. (2016) who modelled the asynchronous growth of the ice complex to its Last Glacial Maximum (LGM) extent. Various lines of geophysical data were used to guide the broad retreat patterns of the modelled ice sheet, including key dating constraints, geomorphological flow sets, notable moraine/grounding

zone wedge positions, and patterns of isostatic loading. An evaluation into the robustness of the optimum deglaciation experiment against these empirical constraints, as well as a detailed analyses of the results, reveal the following insights into the retreat of the EISC:

- Retreat of the ice complex is asynchronous, reflecting regional sensitivities to climate change and various drivers of retreat. Even with increases in bulk precipitation, the Celtic ice sheet diminishes rapidly in response to even modest increases in mean annual air temperature, receding to the Scottish Highlands by 16 ka BP. However, retreat of the marine-based Barents Sea ice sheet is not markedly affected by surface melt, and is instead driven by a combination of reduced mass input (precipitation) and increased rates of calving.
- Independent glacial isostatic modelling shows that the predicted pattern of ice loading matches reasonably well with Late Glacial relative sea level records from across the Eurasian Arctic, particularly over Franz Josef Land, Novaya Zemlya and northern Fennoscandia. Model-empirical misfits are best resolved through regional optimisations of the Earth model. There is support for a low-viscosity zone beneath some regions of the Barents Sea, as proposed in earlier work, but spatial differences in the optimum Earth model may also reflect shortcomings in the ice sheet reconstruction.
- Periodic discharges of icebergs from different regions through the Late Weichselian resonate with numerous observations from the ice-rafted debris record. These include pronounced fluxes at c. 29 ka BP along the western Celtic margin associated with early and rapid expansion of ice in this sector, but also the collapse of the marine-based Barents Sea ice sheet which peaked at 15.2 ka BP with a mass loss rate equivalent to 669 Gt a^{-1}. Total contributions from the EISC to Meltwater Pulse 1A, a short-lived period of dramatic global eustatic sea-level rise coeval with the Bølling warming that exceeded 40 mm per year (14.65-14.31 ka BP; Deschamps et al., 2012), was c. 2.5 metres of sea-level equivalent ice volume.
- During the Younger Dryas, ice caps react differently across the domain. Increased accumulation of ice across the central sectors of the Fennoscandian ice sheet eventually forced a purge of ice through the Gulf of Bothnia at 12.3 ka BP. Reduced bulk precipitation across the Arctic limits any expansion of the remaining ice caps across Svalbard and Russian territories, while a cold-based Scottish ice cap grows rapidly from ice-free conditions within 1 ka.
- The chronology of retreat of Fennoscandian ice through the Baltic and Bothnian seas is a major shortcoming of the model reconstruction, despite an otherwise sound match to the pattern of ice flow history recorded by numerous flowsets. Coupling of the ice model to climate modelling output, for example via PMIP4 (Kageyama et al., 2016), may potentially resolve such discrepancies in the deglacial mass balance regime, and is an area worthy of future inspection.
- The large Baltic and White Sea proglacial lakes form expanded rapidly after retreat of the FIS during the Bølling/Allerød transition, and persisted through the Younger Dryas stadial capturing surface runoff from a combined coverage of 12.9 x 10^5 km^2 of the Eurasian continent at this time.
- Hydrological routing beneath the LGM ice complex reveal 6,143 potential subglacial lake locations across a variety of glaciological settings, with the distribution heavily skewed to surface areas <= 10 km^2. The largest lake lies in the Gulf of Bothnia, beneath a zone of prominent ice streaming from the Fennoscandian ice sheet, and in combination with a proliferation of smaller lakes thus likely formed a major control on its dynamic behaviour.
- Catchment areas for the major Eurasian rivers were heavily affected by the presence of the EISC as well as eustatic sea level lowering, with the Fleuve Manche river catchment dominating the LGM European geography. Its catchment area exceeded 2.5 × 10^6 km^2, including the drainage of meltwater runoff from one quarter of the ice complex. The discharge for such a river system,

sensitive to periodic meltwater injections triggered by ice sheet fluctuations, was a probable driver for North Atlantic circulation perturbations for much of the glaciation.

Acknowledgements

The research is part of the Centre for Arctic Gas Hydrate, Environment and Climate, and was supported by the Research Council of Norway through its Centres of Excellence funding scheme (grant 223259), the PetroMaks project “Glaciations in the Barents Sea area (GlaciBar)” (grant 200672), and a Stockholm Uni SUCLIM consortium grant (to Stroeven) that supported Hubbard in the early development of the model code. We thank two anonymous reviewers for their constructive feedback to improve the manuscript.

Figure captions

Figure 1: Major drainage routes of the Eurasian ice sheet complex, adapted from Stokes and Clark (2001), Ottesen et al. (2005) and Clark et al. (2012). Locations of major trough mouth fans (brown) adapted from Dahlgren et al. (2005) and Batchelor and Dowdeswell (2014). BDF: Barra and Donegal Fans; RB: Rosemary Bank; NSF: North Sea Fan; Bj: Bjørnøyrenna Fan. Glacial limits are compiled from Ehlers and Gibbard (2007), Patton et al. (2015) and Stroeven et al. (2016). Recent evidence for the extension of the Celtic ice sheet onto Porcupine Bank (Peters et al., 2015) and in the southern Celtic Sea are also incorporated (Praeg et al., 2015).

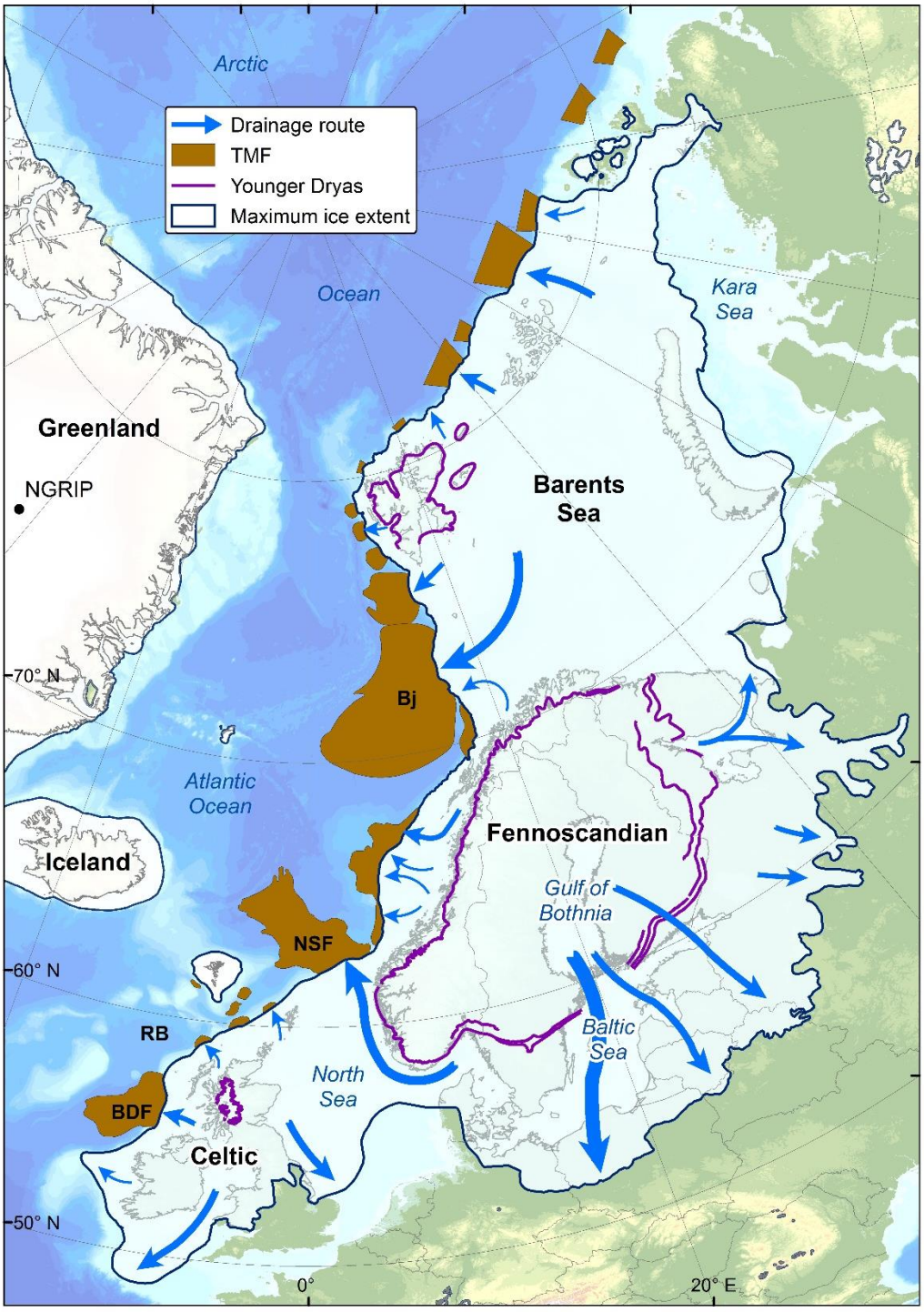

Figure 2: Forcing curves used to drive the evolution of the optimum EISC deglaciation experiment (23-8 ka BP), with bulk changes in climate forcing and calving sensitivity tuned separately for the three sub-domains of the complex. A) Eustatic sea level forcing (Waelbroeck et al., 2002); B) Mean annual air temperature (MAAT) forcing curves used to drive the deglaciation experiments, scaled against the NGRIP $\delta^{18}O$ record (Andersen et al., 2004), C) Transient changes in total precipitation (relative to present day levels) across the three sub domains of the ice complex; D) Transient changes in the sensitivity to calving losses, with higher values leading to increased calving losses along a linear relationship. Arctic areas are defined as being above 78°N. Chronozones marked include the Bølling/Allerød (Bø-Al) oscillation (14.6 – 12.9 ka BP) and Younger Dryas (YD) stadial (12.9 – 11.7 ka BP).

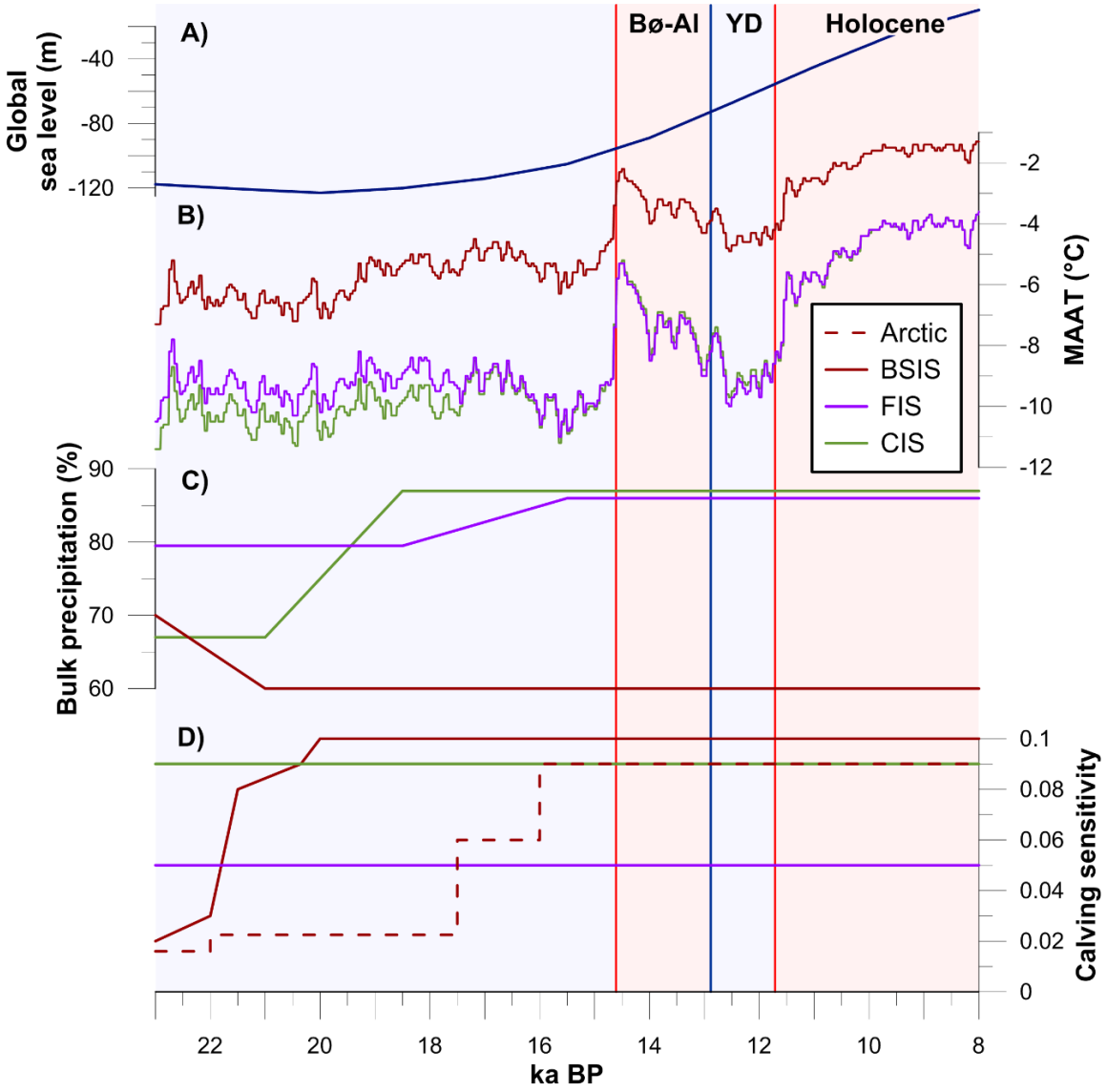

Figure 3: Areal and volumetric changes for the three semi-independent ice sheet components of EISC through the full Late Weichselian, extending the optimum build-up (37-19 ka BP) experiment of Patton et al. (2016). Acronyms used: CIS (Celtic ice sheet); FIS (Fennoscandian ice sheet); and BSIS (Barents Sea ice sheet). Note the log scale for CIS ice volume. Chronozones marked include the Bølling/Allerød (Bø-Al) oscillation (14.6 – 12.9 ka BP) and Younger Dryas (YD) stadial (12.9 – 11.7 ka BP).

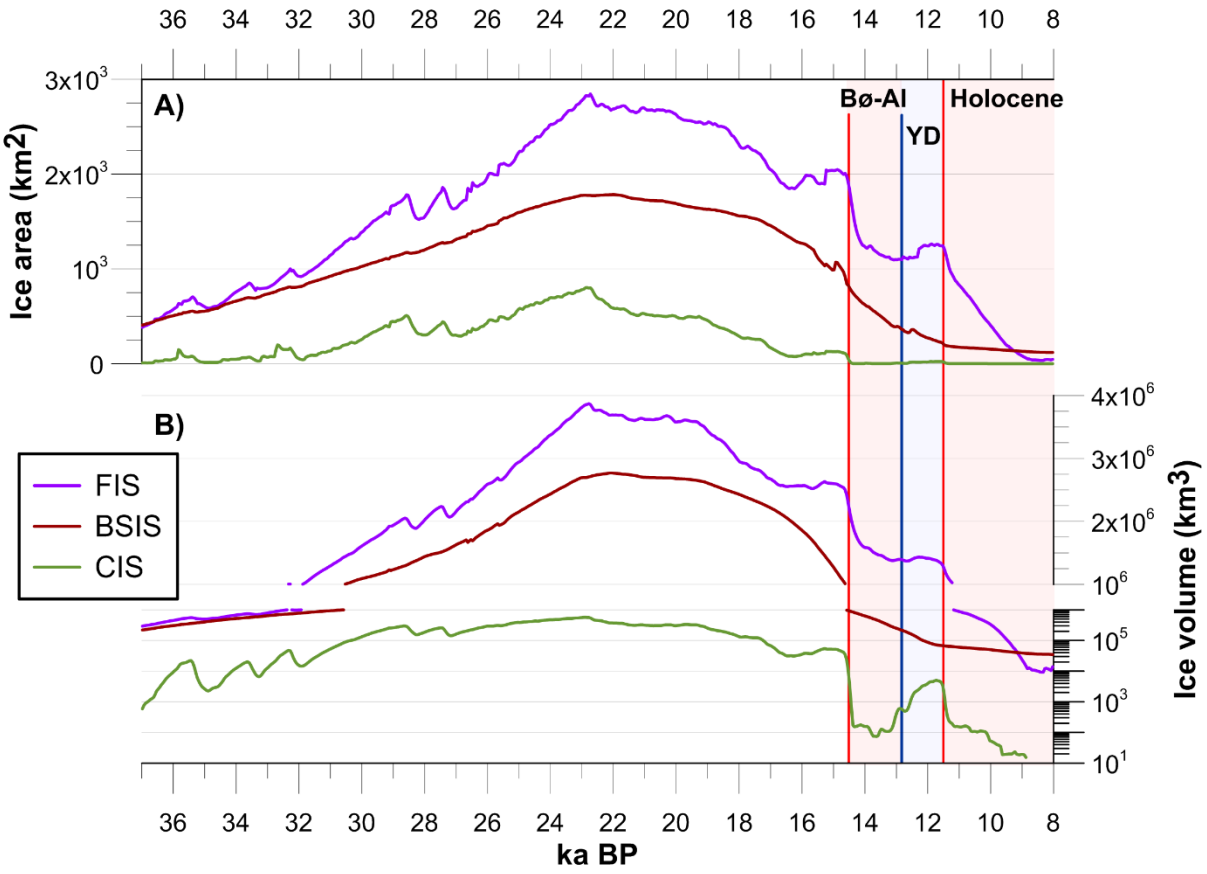

Figure 4: Timeslices showing ice extent and ice-surface velocities during deglaciation of the Eurasian ice sheet complex 20-10 ka. Surface elevation contours are drawn every 250 m. Sea level is determined from the global sea level forcing curve (Figure 3A) and includes corrections based on modelled isostatic loading effects. Black polygons indicate empirically derived maximum limits of EISC glaciation for 20, 18, 17, 16, 15, 14, 13, and 10 ka for panels A-H, respectively (Hughes et al., 2016). Shorelines of major proglacial lakes are defined based on the elevation of the contemporary sea level position. Acronyms used: G – Göteborg Moraine; HC – Halland Coastal Moraine; SoH – Sea of Hebrides

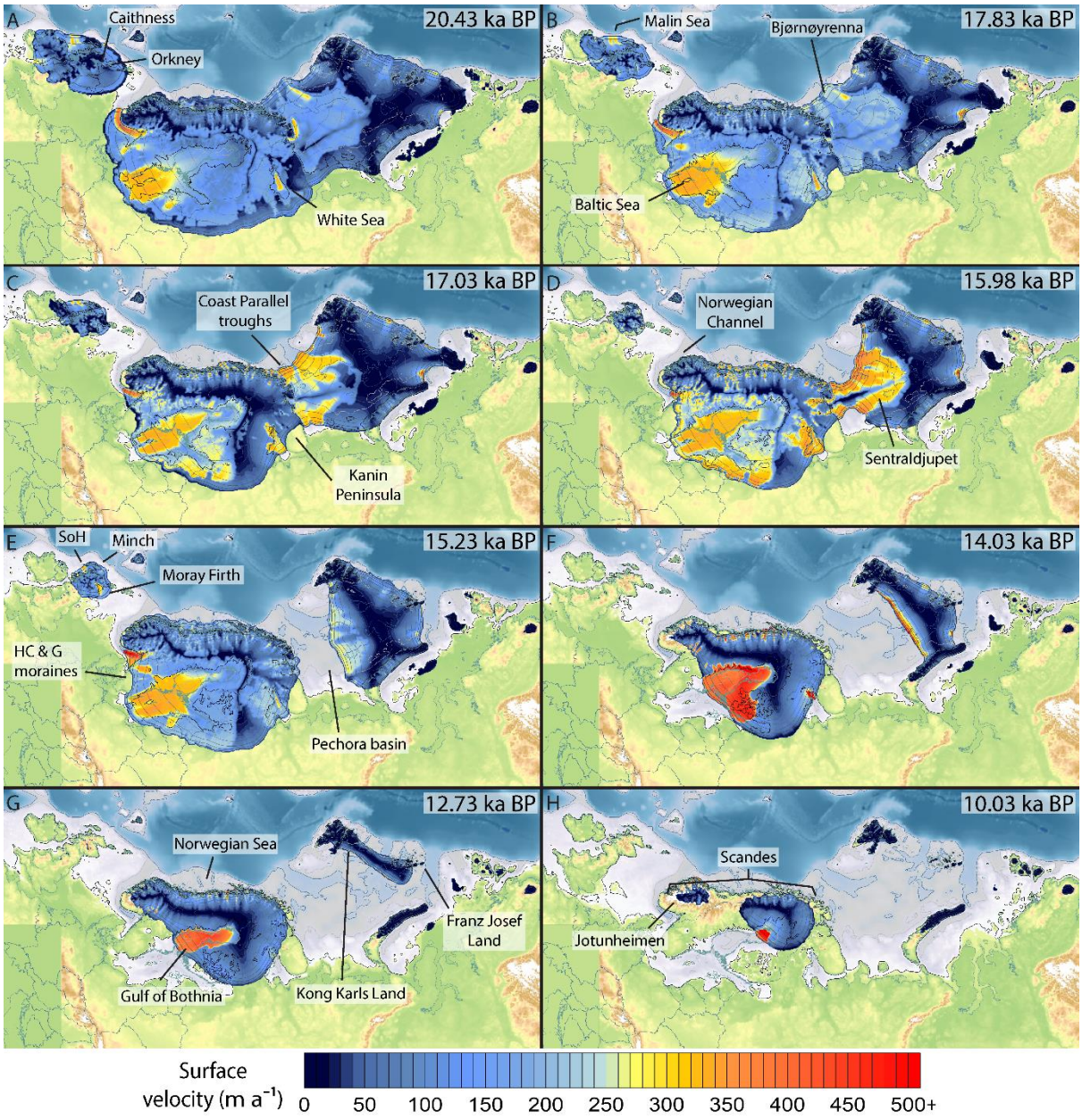

Figure 5: Comparisons between relative sea level (RSL) data and model predictions for 5 locations representative of the four regions – Franz Josef Land (FJL), Novaya Zemlya (NZ), northern Fennoscandia (Fe), and Svalbard (Sv). The black symbols and error bars show the empirical observations, with the black dashed line giving the elevation of the highest marine limit. The UiT_2016 model data (pink) refers to an earlier published iteration of the modelled deglaciation wherein ice retreat was more loosely constrained (Auriac et al., 2016).

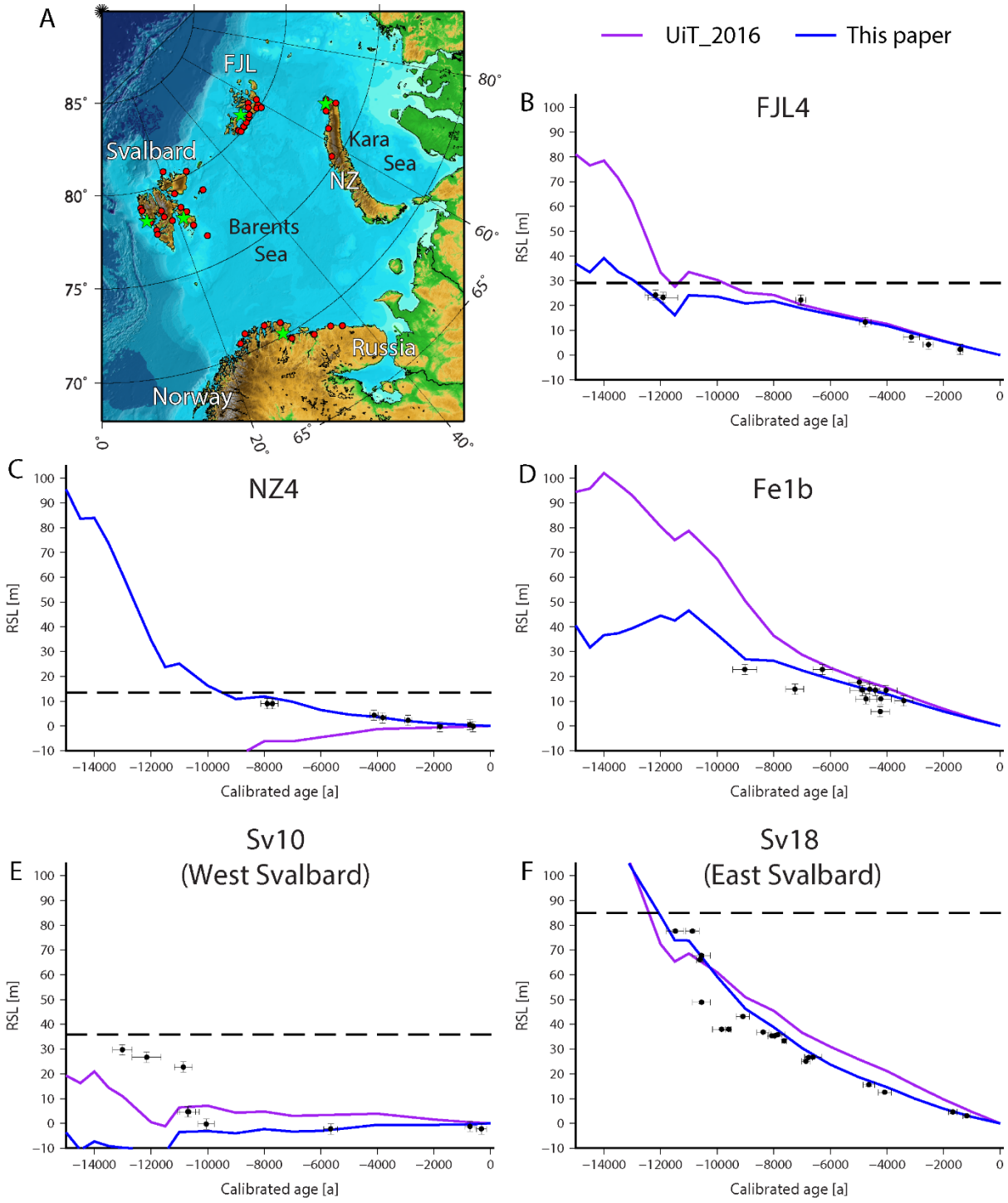

Figure 6: Comparison of the optimum deglaciation scenario with empirically based conceptual models across Fennoscandia. Deglacial flow sets (red and green) are drawn according to landform mapping carried out by Kleman et al. (1997). A) An abridged deglaciation pattern and chronology ≤17 ka BP according to Stroeven et al. (2016), where ice margins were predominantly reconstructed transverse to the youngest documented flow traces (e.g., eskers), marginal meltwater channels, and ice-dammed lakes. B) Retreat pattern and chronology of the optimum deglaciation scenario from this study, including the maximum Younger Dryas extent at 11.7 ka BP. C) An abridged version of the "most-credible" 1 ka timeslice reconstruction ≤19 ka BP by Hughes et al. (2016), with limits drawn based on the distribution and ages of published numerical dates in the DATED-1 database. Acronyms used: HCM – Halland Coastal Moraines; NCIS – Norwegian Channel ice stream; U – Utsira; Å-V – Ångermanland-Västerbotten coastline.

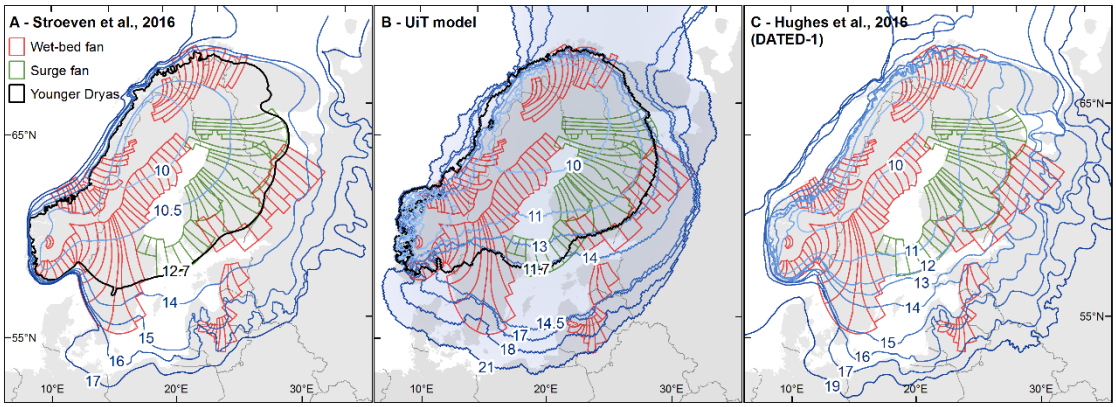

Figure 7: Interpolated and modelled ages of deglaciation from A) the FIS timeslice reconstruction by Stroeven et al. (2016); B) the optimum deglaciation scenario of this paper, and C) the "most credible" 1 ka timeslice reconstruction based from the DATED-1 database by Hughes et al. (2016). The age of maximum Younger Dryas extents vary from 12.7 ka BP (A) to 11.73 ka BP (B).

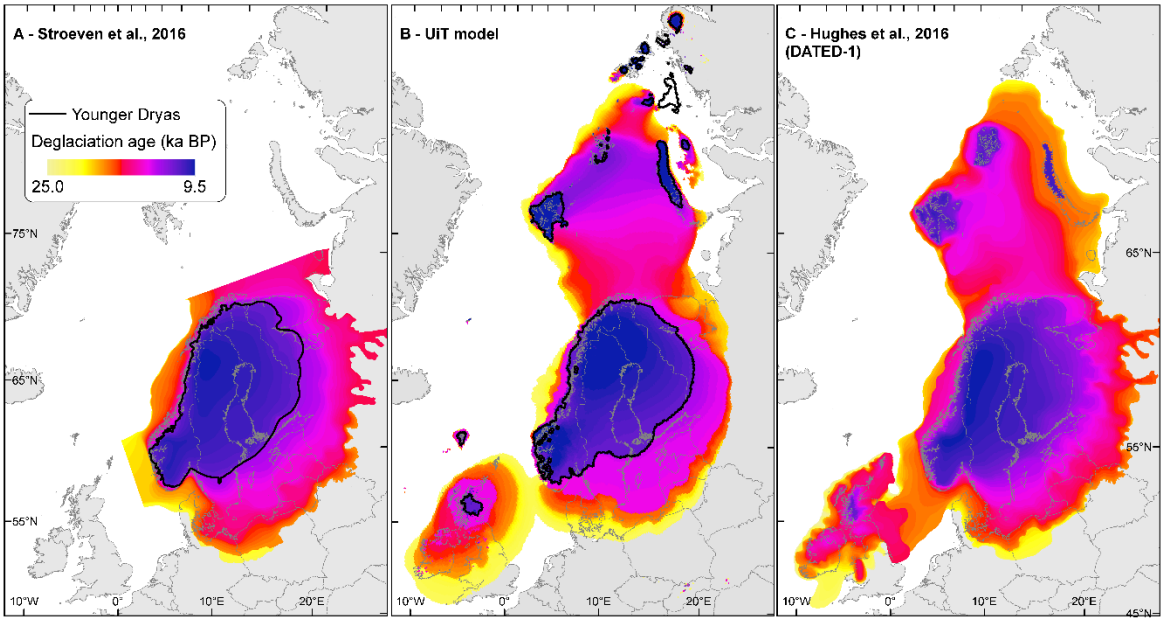

Figure 8: A) Mapped glacial landforms offshore in the southern Barents Sea, with flowset grouping and numbering as interpreted by Winsborrow et al. (2010). B-D) Residual differences (Li et al., 2007; Napieralski et al., 2007) between modelled flow vectors and lineation directions through the Late Weichselian for three sub-regions: Lower Bjørnøyrenna (B); Finnmark coastline (C); and NW Norway (D). Interpreted ages based on relative positioning of the flowsets taken from Winsborrow et al. (2010) are given in brackets. In the absence of absolute chronological dating, "LGM" flowsets refer to a more general time of expansive glaciation prior to deglaciation, with subsequent retreat stages determined based on dated grounding zone wedges (Figure 12 - Patton et al., 2015).

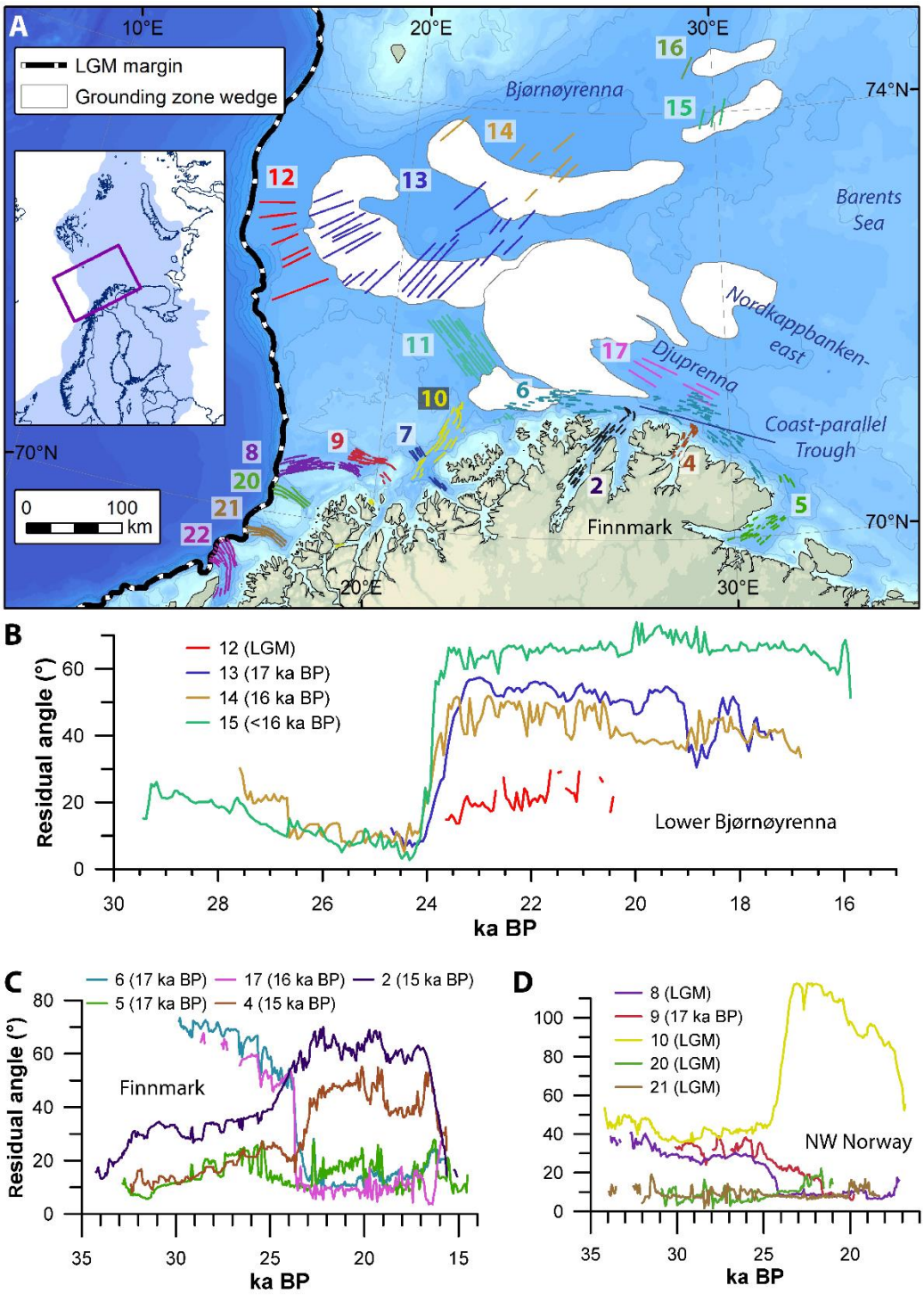

Figure 9: A) Major interruptions in retreat of the modelled EISC during the Late Weichselian. B) Margins are identified on the basis that they are not subsequently overriden by ice. Large gaps between pauses in margin retreat are indicitive of the rapid withdrawal of ice. Acronyms used: KG – Kandalaksha Gulf; IS – Irish Sea.

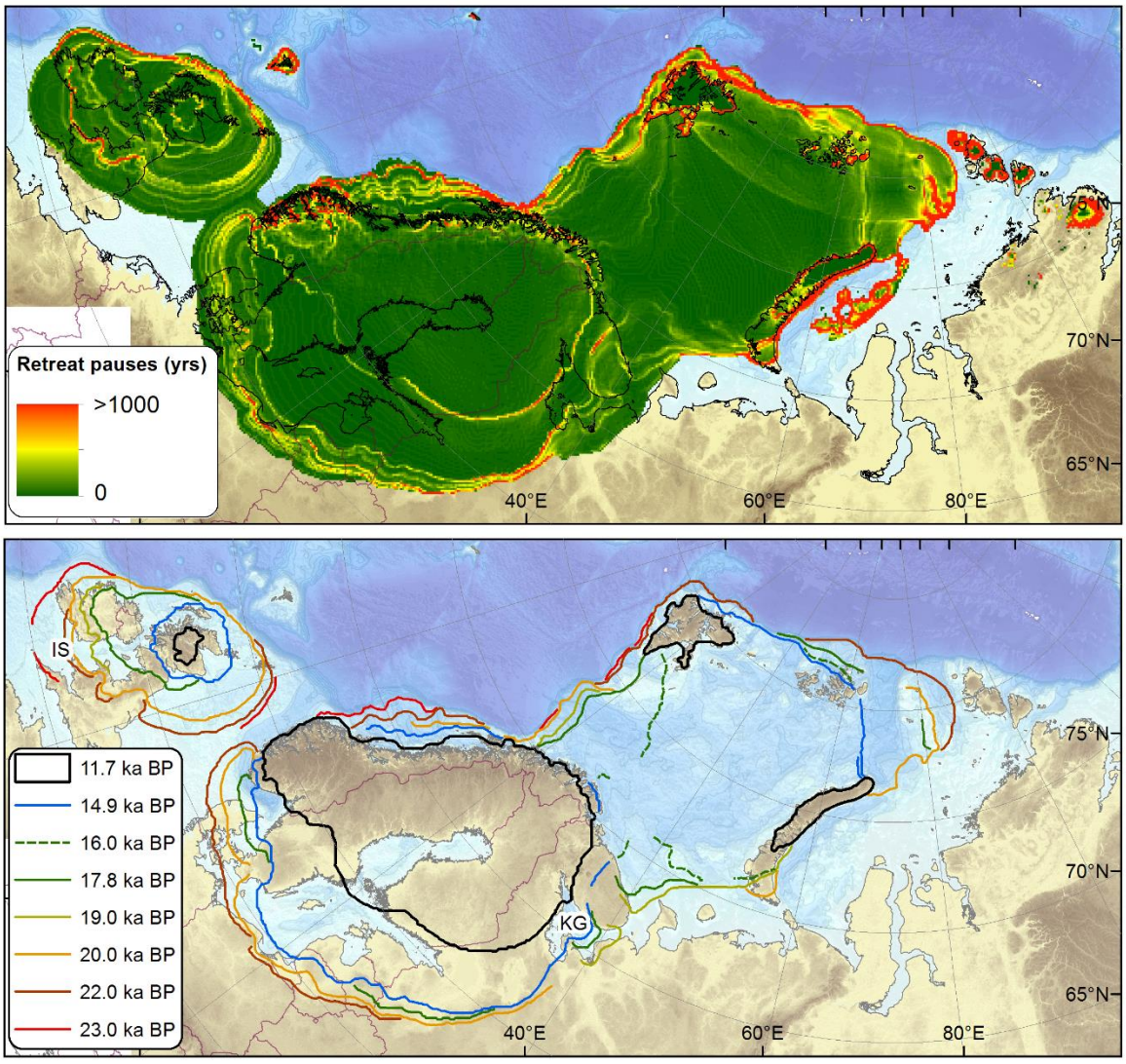

Figure 10: Surface melting and calving flux variations from selected regions of the EISC through the Late Weichselian and Early Holocene (cf. Patton et al., 2016). Regions are defined based on the broad positions of the main ice divides at the LGM (22.73 ka BP). Mass loss values refer to region-wide averages. Locations of major trough mouth fans (brown) adapted from Dahlgren et al. (2005) and Batchelor and Dowdeswell (2014). BDF: Barra and Donegal Fans; RB: Rosemary Bank.

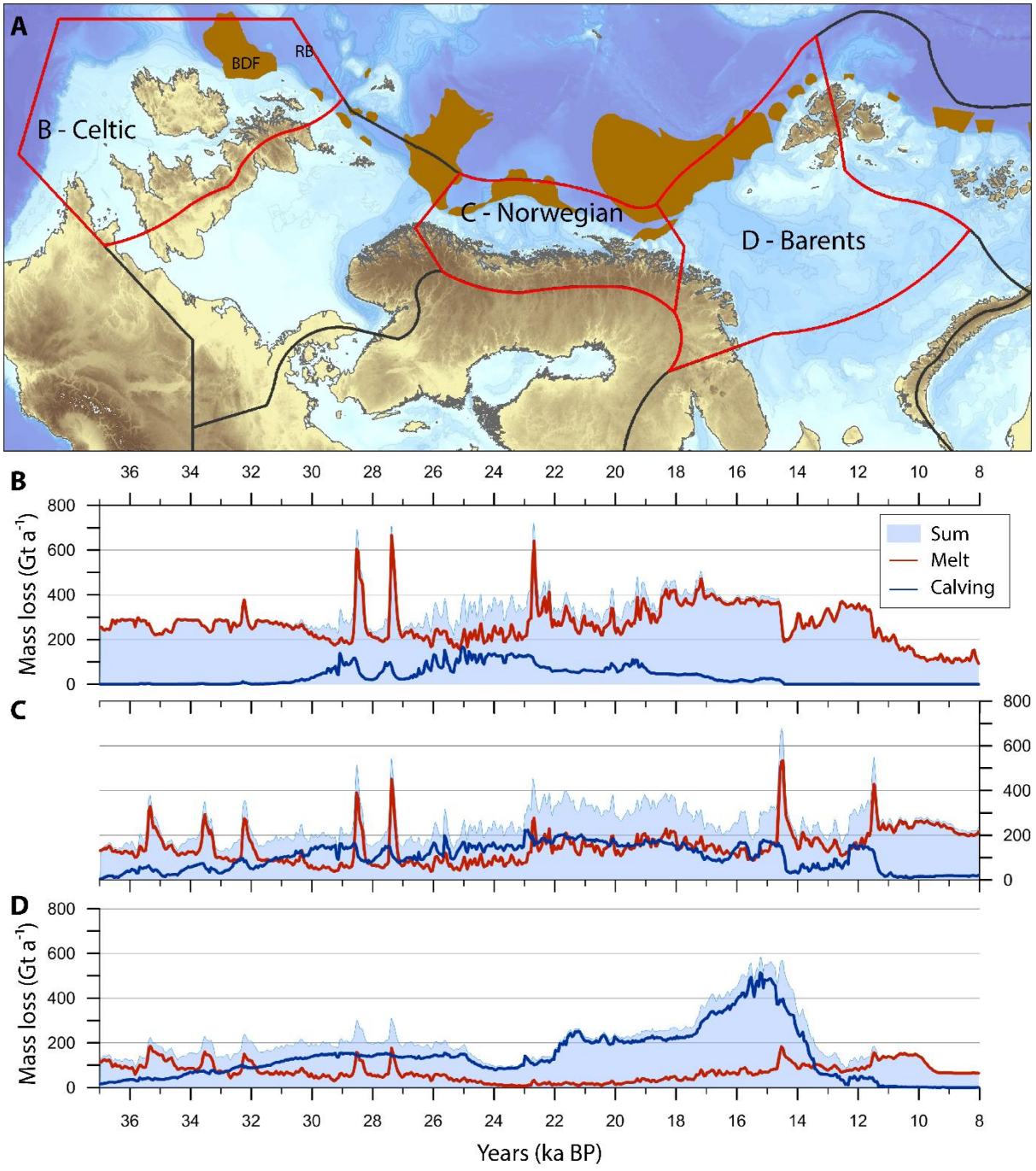

Figure 11: A) Present day bathymetry of the Barents and Kara seas overlain by the main ocean currents (modified from Gammelsrød et al. (2009)). FV: Franz Victoria trough; SA: Saint Anna trough. B) Modelled bathymetry across the Barents and Kara seas at 12 ka BP, taking into account changes in relative sea level due to glacial isostatic adjustment and drops in eustatic sea level.

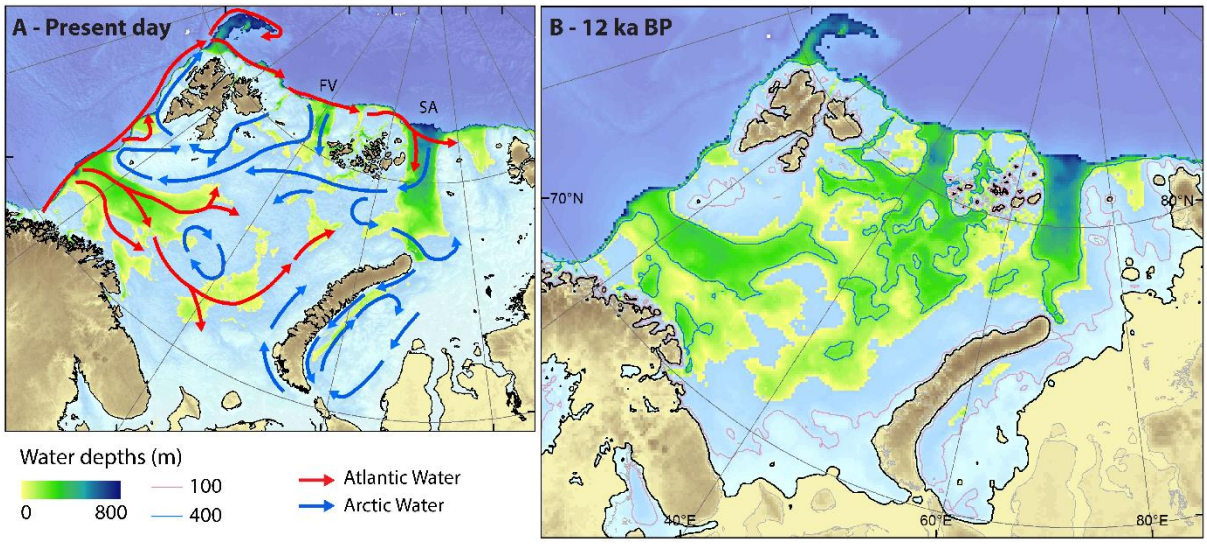

Figure 12: The distribution of 6,143 potential subglacial lake locations beneath the LGM EISC. A number of key assumptions will affect the under- and over-prediction of these lake locations, including use of an initial elevation model draped with (post-) glacial sediments and bodies of freshwater, a lack of dynamic coupling between ice and subglacial meltwater, and the treatment of the bed as being entirely warm-based. Water routing and filling of the basal hydraulic potential surface was carried out using Arc Hydro Tools for ArcGIS 10.3. The elevation model used is an isostatically adjusted and resampled version of the GEBCO_2014 Grid at 500 m resolution, with glacial isostatic effects derived from the coupled elastic lithosphere/relaxed asthenosphere scheme of the ice model. Lakes with a surface area <2 km^2 were discarded from this analysis. Acronyms used: Se – Sentralbanken; St – Storbanken.

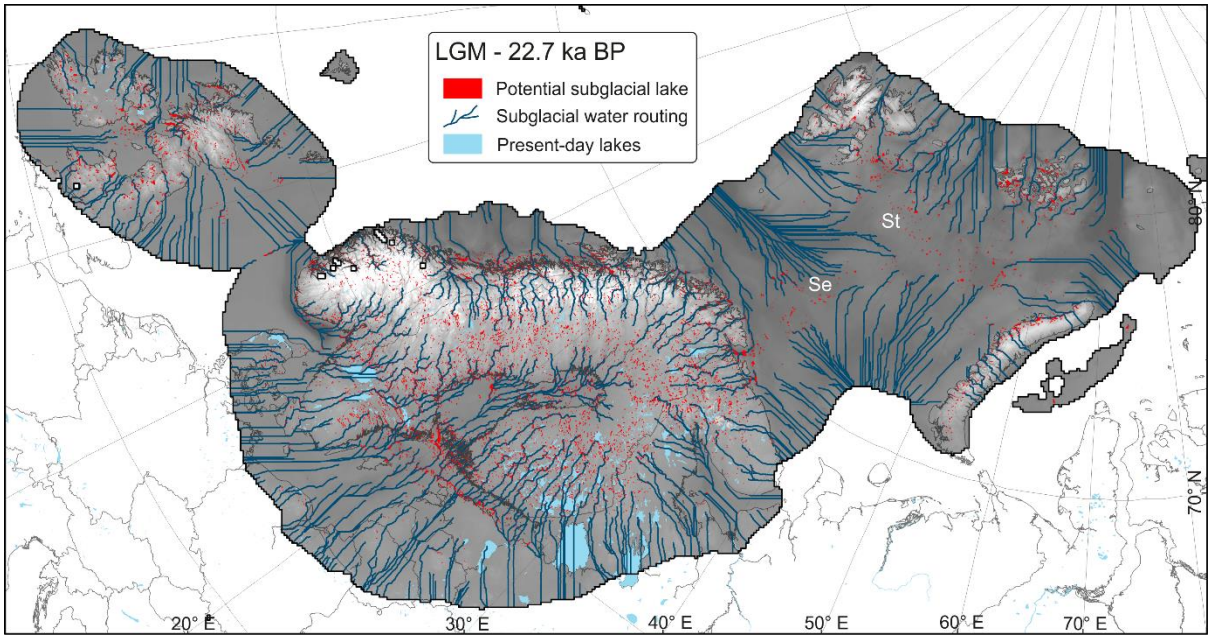

Figure 13: The potential Fleuve Manche catchment during the Last Glacial Maximum at 22.73 ka BP, when the Celtic (CIS), Fennoscandian (FIS) ice sheets were coalesced and around their peak extents (Patton et al., 2016). Over half of its basin (53 %) was ice-covered, draining meltwater from CIS, FIS, and Alpine ice sheets. Water routing, lake formation, and catchment delineation analyses was carried out using Arc Hydro Tools for ArcGIS 10.3. The elevation model used is an isostatically adjusted and resampled version of the GEBCO_2014 Grid at 500 m resolution, with glacial isostatic effects derived from the coupled elastic lithosphere/relaxed asthenosphere scheme of the ice model.

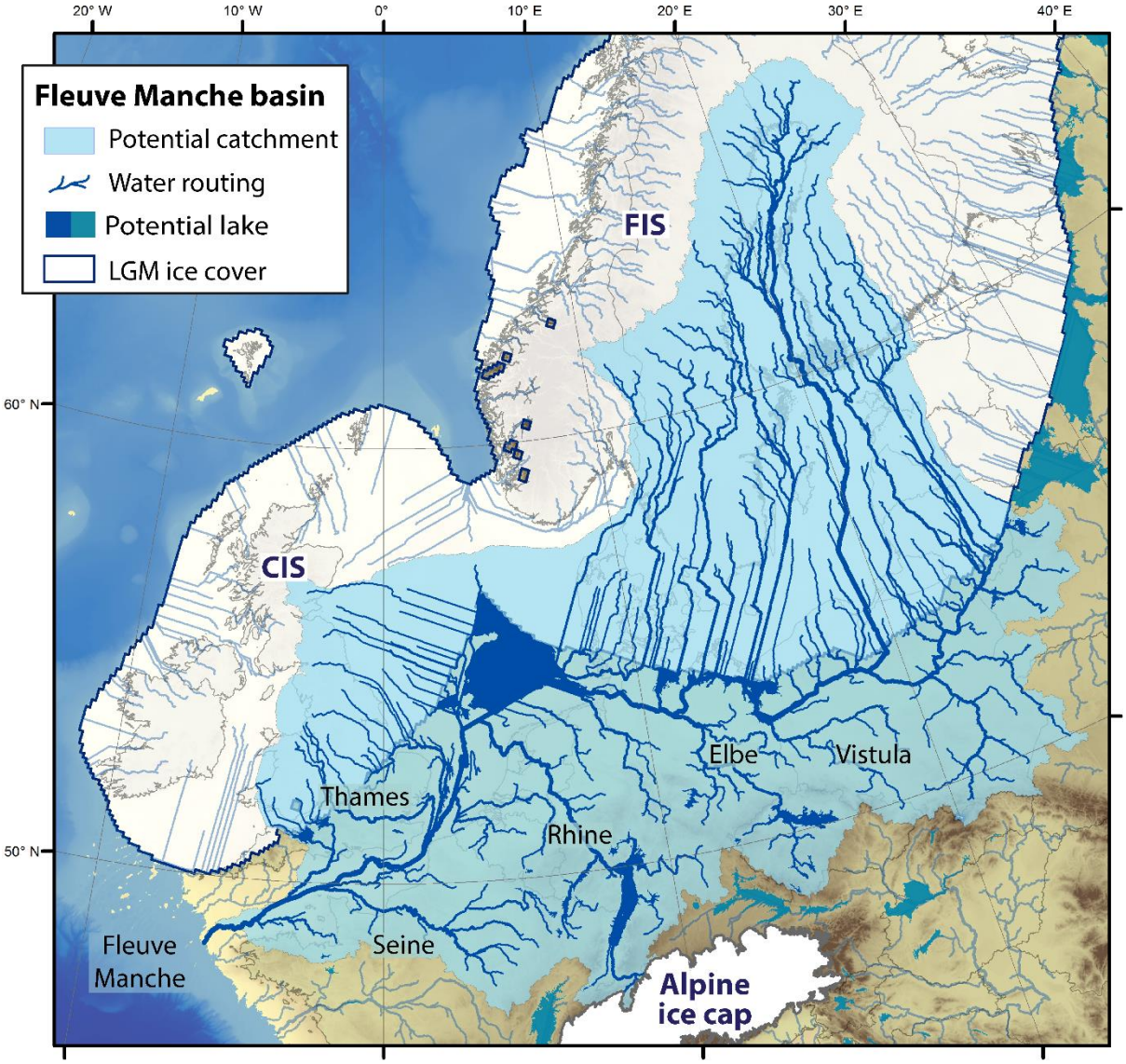

Figure 14: The peak glacial extent during the Younger Dryas stadial compared to empirically derived limits (red line; Stroeven et al., 2016). During this brief interstadial the Baltic and White Sea ice lakes were major components of the proglacial hydrological system, damming Eurasian river drainage and surface melt fluxes from the Fennoscandian ice sheet. Their outlets were c. 24 and 23 m above contemporaneous sea level, respectively. Mount Billingen (MB) is the commonly attributed spill point for the Baltic Ice Lake at c. 25 m above contemporaneous sea level (e.g., Stroeven et al., 2015). Surface areas of the two lakes total 321,715 and 55,610 km^2, respectively (Table 2). Catchment areas (not including glacial sources) total 4.97 x 10^5 km^2 for the Fleuve Manche River in the English Channel (orange), 9.26 x 10^5 km^2 for the Baltic Ice Lake (yellow), and 3.61 x 10^5 km^2 for the White Sea Ice Lake (green; Table 2). The contemporary continental river network (blue lines) was calculated using Arc Hydro Tools for ArcGIS 10.3.

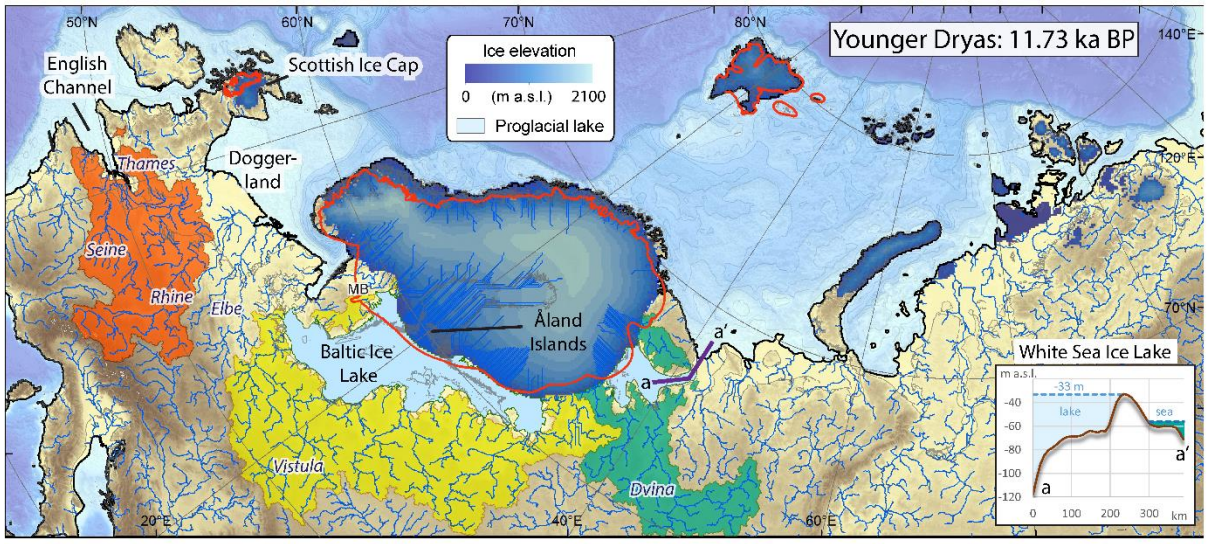

Figure S1.: Comparisons between relative sea level (RSL) data and model predictions from this study (blue) for the four regions – A) Svalbard (Sv); B) Franz Josef Land (FJL); C) Novaya Zemlya (NZ); and D) northern Fennoscandia (Fe). The black symbols and error bars show the empirical observations, with the black dashed line giving the elevation of the highest marine limit. The UiT_2016 model data (pink) refers to an earlier published iteration of the modelled deglaciation wherein ice retreat was more loosely constrained (Auriac et al., 2016).

Table captions

Table 1: χ^2 and best-fitting Earth rheology parameters for regional fits of the optimum reconstruction, compared with an earlier and less well-constrained model experiment (UiT_2016) of the deglaciation presented by Auriac et al. (2016). Parameters include: *h* (lithosphere thickness – km), v_u (upper mantle viscosity – 10^{21} Pa s), and v_l (lower mantle viscosity – 10^{21} Pa s).

Model	Svalbard (n = 18)				Franz Josef Land (n = 13)				Novaya Zemlya (n = 6)				Northern Fennoscandia (n = 9)			
	χ_g^2	h	v_u	v_l	χ_g^2	h	v_u	v_l	χ_g^2	h	v_u	v_l	χ_g^2	h	v_u	v_l
UiT_2016	20.6	120	0.2	2	2.5	96	3	20	0.4	120	0.05	3	51.9	120	5	50
This paper	75.3	120	1	1	3.1	120	3	10	0.3	120	0.2	1	8.1	120	2	20

Model	Svalbard (East)* (n = 11)				Global (n = 46)			
	χ_g^2	h	v_u	v_l	χ_g^2	h	v_u	v_l
UiT_2016	-	-	-	-	66.6	120	2	50
This paper	48.0	96	0.3	2	77.9	71	0.2	1

Table 2: Dimensions and capacities of major hydrographic features of the Eurasian domain during the last glacial cycle. Younger Dryas catchment areas for the Baltic Ice Lake and White Sea Ice Lake concern their paraglacial portions only.

	Lake area km^2	Lake volume km^3	Basin area 10^5 km^2
Last Glacial Maximum			
Fleuve Manche palaeoriver	-	-	25.58
(of which subglacial)	-	-	13.62
(of which paraglacial)	-	-	11.96
Younger Dryas			
Fleuve Manche palaeoriver	-	-	4.97
Baltic Ice Lake	321,715	23,464	9.26
White Sea Ice Lake	55,610	4,171	3.61

References

Andersen, B.G., Lundqvist, J., Saarnisto, M., 1995. The Younger Dryas margin of the Scandinavian Ice Sheet — An introduction. Quat. Int. 28, 145–146. doi:10.1016/1040-6182(95)00043-I

Andersen, K.K., Azuma, N., Barnola, J.-M., Bigler, M., Biscaye, P., Caillon, N., Chappellaz, J., Clausen, H.B., Dahl-Jensen, D., Fischer, H., Flückiger, J., Fritzsche, D., Fujii, Y., Goto-Azuma, K., Grønvold, K., Gundestrup, N.S., Hansson, M., Huber, C., Hvidberg, C.S., Johnsen, S.J., Jonsell, U., Jouzel, J., Kipfstuhl, S., Landais, A., Leuenberger, M., Lorrain, R., Masson-Delmotte, V., Miller, H., Motoyama, H., Narita, H., Popp, T., Rasmussen, S.O., Raynaud, D., Rothlisberger, R., Ruth, U., Samyn, D., Schwander, J., Shoji, H., Siggard-Andersen, M.-L., Steffensen, J.P., Stocker, T., Sveinbjörnsdóttir, a E., Svensson, A., Takata, M., Tison, J.-L., Thorsteinsson, T., Watanabe, O., Wilhelms, F., White, J.W.C., 2004. High-resolution record of Northern Hemisphere climate extending into the last interglacial period. Nature 431, 147–151. doi:10.1038/nature02805

Andreassen, K., Hubbard, A., Winsborrow, M.C.M., Patton, H., Vadakkepuliyambatta, S., Plaza-Faverola, A., Gudlaugsson, E., Serov, P., Deryabin, A., Mattingsdal, R., Mienert, J., Bünz, S., n.d. Massive blow-out craters formed by hydrate-controlled methane expulsion from the Arctic seafloor. Science.

Andreassen, K., Winsborrow, M.C.M., Bjarnadóttir, L.R., Rüther, D.C., 2014. Ice stream retreat dynamics inferred from an assemblage of landforms in the northern Barents Sea. Quat. Sci. Rev. 92, 246–257. doi:10.1016/j.quascirev.2013.09.015

Andrén, T., Lindeberg, G., Andrén, E., 2002. Evidence of the final drainage of the Baltic Ice Lake and the brackish phase of the Yoldia Sea in glacial varves from the Baltic Sea. Boreas 31, 226–238. doi:10.1111/j.1502-3885.2002.tb01069.x

Arnold, N., Sharp, M., 2002. Flow variability in the Scandinavian ice sheet: modelling the coupling between ice sheet flow and hydrology. Quat. Sci. Rev. 21, 485–502. doi:10.1016/S0277-3791(01)00059-2

Auriac, A., Whitehouse, P.L., Bentley, M.J., Patton, H., Lloyd, J.M., Hubbard, A.L., 2016. Glacial isostatic adjustment associated with the Barents Sea ice sheet: a modelling inter-comparison. Quat. Sci. Rev. 147, 122–135. doi:10.1016/j.quascirev.2016.02.011

Austin, W.E.., Kroon, D., 2001. Deep sea ventilation of the northeastern Atlantic during the last 15,000 years. Glob. Planet. Change 30, 13–31. doi:10.1016/S0921-8181(01)00074-1

Ballantyne, C.K., 2010. Extent and deglacial chronology of the last British-Irish Ice Sheet: implications of exposure dating using cosmogenic isotopes. J. Quat. Sci. 25, 515–534. doi:10.1002/jqs.1310

Banwell, A.F., Willis, I.C., Arnold, N.S., 2013. Modeling subglacial water routing at Paakitsoq, W Greenland. J. Geophys. Res. Earth Surf. 118, 1282–1295. doi:10.1002/jgrf.20093

Batchelor, C.L., Dowdeswell, J.A., 2014. The physiography of High Arctic cross-shelf troughs. Quat. Sci. Rev. 92, 68–96. doi:10.1016/j.quascirev.2013.05.025

Bell, R.E., Studinger, M., Shuman, C.A., Fahnestock, M.A., Joughin, I., 2007. Large subglacial lakes in East Antarctica at the onset of fast-flowing ice streams. Nature 445, 904–907. doi:10.1038/nature05554

Bennett, M.R., Boulton, G.S., 1993. Deglaciation of the Younger Dryas or Loch-Lomond Stadial Ice-Field in the Northern Highlands, Scotland. J. Quat. Sci. 8, 133–145. doi:10.1002/jqs.3390080206

Bentley, M.J., Ó Cofaigh, C., Anderson, J.B., Conway, H., Davies, B., Graham, A.G.C., Hillenbrand, C.-D., Hodgson, D.A., Jamieson, S.S.R., Larter, R.D., Mackintosh, A., Smith, J.A., Verleyen, E.,

Ackert, R.P., Bart, P.J., Berg, S., Brunstein, D., Canals, M., Colhoun, E.A., Crosta, X., Dickens, W.A., Domack, E., Dowdeswell, J.A., Dunbar, R., Ehrmann, W., Evans, J., Favier, V., Fink, D., Fogwill, C.J., Glasser, N.F., Gohl, K., Golledge, N.R., Goodwin, I., Gore, D.B., Greenwood, S.L., Hall, B.L., Hall, K., Hedding, D.W., Hein, A.S., Hocking, E.P., Jakobsson, M., Johnson, J.S., Jomelli, V., Jones, R.S., Klages, J.P., Kristoffersen, Y., Kuhn, G., Leventer, A., Licht, K., Lilly, K., Lindow, J., Livingstone, S.J., Massé, G., McGlone, M.S., McKay, R.M., Melles, M., Miura, H., Mulvaney, R., Nel, W., Nitsche, F.O., O'Brien, P.E., Post, A.L., Roberts, S.J., Saunders, K.M., Selkirk, P.M., Simms, A.R., Spiegel, C., Stolldorf, T.D., Sugden, D.E., van der Putten, N., van Ommen, T., Verfaillie, D., Vyverman, W., Wagner, B., White, D.A., Witus, A.E., Zwartz, D., 2014. A community-based geological reconstruction of Antarctic Ice Sheet deglaciation since the Last Glacial Maximum. Quat. Sci. Rev. 100, 1–9. doi:10.1016/j.quascirev.2014.06.025

Berger, A., Loutre, M.F., 1991. Insolation values for the climate of the last 10 million years. Quat. Sci. Rev. 10, 297–317. doi:10.1016/0277-3791(91)90033-Q

Birgel, D., Hass, H., 2004. Oceanic and atmospheric variations during the last deglaciation in the Fram Strait (Arctic Ocean): a coupled high-resolution organic-geochemical and sedimentological study. Quat. Sci. Rev. 23, 29–47. doi:10.1016/j.quascirev.2003.10.001

Bischof, J.F., 1994. The decay of the Barents ice sheet as documented in nordic seas ice-rafted debris. Mar. Geol. 117, 35–55. doi:10.1016/0025-3227(94)90005-1

Bjarnadóttir, L.R., Winsborrow, M.C.M., Andreassen, K., 2016. Large subglacial meltwater features in the central Barents Sea. Geology 45, 159–163. doi:10.1111/bor.12142

Bjarnadóttir, L.R., Winsborrow, M.C.M., Andreassen, K., 2014. Deglaciation of the central Barents Sea. Quat. Sci. Rev. 92, 208–226. doi:10.1016/j.quascirev.2013.09.012

Björck, S., 2008. The late Quaternary development of the Baltic Sea, in: Team, B.A. (Ed.), Assessment of Climate Change for the Baltic Sea Basin. Springer Verlag, Berlin, Heidelberg, pp. 398–407.

Blake, W., 1961. Radiocarbon dating of raised beaches in Nordaustlandet, Spitsbergen, in: Geology of the Arctic: Proceedings of the First International Symposium on Arctic Geology. University of Toronto Press, Toronto, pp. 133–145.

Blatter, H., 1995. Velocity and stress-fields in grounded glaciers - a simple algorithm for including deviatoric stress gradients. J. Glaciol. 41, 333–344. doi:10.3198/1995JoG41-138-333-344

Bodén, P., Fairbanks, R.G., Wright, J.D., Burckle, L.H., 1997. High-resolution stable isotope records from southwest Sweden: The drainage of the Baltic Ice Lake and Younger Dryas Ice Margin Oscillations. Paleoceanography 12, 39–49. doi:10.1029/96PA02879

Boulton, G., Hagdorn, M., 2006. Glaciology of the British Isles Ice Sheet during the last glacial cycle: form, flow, streams and lobes. Quat. Sci. Rev. 25, 3359–3390. doi:10.1016/j.quascirev.2006.10.013

Boulton, G.S., Dongelmans, P.W., Punkari, M., Broadgate, M., 2001. Palaeoglaciology of an ice sheet through a glacial cycle: the European ice sheet through the Weichselian. Quat. Sci. Rev. 20, 591–625. doi:10.1016/S0277-3791(00)00160-8

Bradwell, T., Stoker, M.S., Golledge, N.R., Wilson, C.K., Merritt, J.W., Long, D., Everest, J.D., Hestvik, O.B., Stevenson, A.G., Hubbard, A.L., Finlayson, A.G., Mathers, H.E., 2008. The northern sector of the last British Ice Sheet: Maximum extent and demise. Earth-Science Rev. 88, 207–226. doi:10.1016/j.earscirev.2008.01.008

Briner, J.P., Goehring, B.M., Mangerud, J., Svendsen, J.I., 2016. The deep accumulation of 10Be at Utsira, southwestern Norway: Implications for cosmogenic nuclide exposure dating in

peripheral ice sheet landscapes. Geophys. Res. Lett. 43, 9121–9129. doi:10.1002/2016GL070100

Bromley, G.R.M., Putnam, A.E., Rademaker, K.M., Lowell, T. V, Schaefer, J.M., Hall, B., Winckler, G., Birkel, S.D., Borns, H.W., 2014. Younger Dryas deglaciation of Scotland driven by warming summers. Proc. Natl. Acad. Sci. U. S. A. 111, 6215–6219. doi:10.1073/pnas.1321122111

Brown, C.S., Meier, M.F., Post, A., 1982. Calving speed of Alaskan tidewater glaciers, with application to Columbia Glacier, US Geological Survey Professional Paper 1258-C.

Chauhan, T., Rasmussen, T.L., Noormets, R., Jakobsson, M., Hogan, K.A., 2014. Glacial history and paleoceanography of the southern Yermak Plateau since 132 ka BP. Quat. Sci. Rev. 92, 155–169. doi:10.1016/j.quascirev.2013.10.023

Chiverrell, R.C., Thrasher, I.M., Thomas, G.S.P., Lang, A., Scourse, J.D., van Landeghem, K.J.J., McCarroll, D., Clark, C.D., Cofaigh, C.Ó., Evans, D.J.A., Ballantyne, C.K., 2013. Bayesian modelling the retreat of the Irish Sea Ice Stream. J. Quat. Sci. 28, 200–209. doi:10.1002/jqs.2616

Christoffersen, P., Tulaczyk, S., Wattrus, N.J., Peterson, J., Quintana-Krupinski, N., Clark, C.D., Sjunneskog, C., 2008. Large subglacial lake beneath the Laurentide Ice Sheet inferred from sedimentary sequences. Geology 36, 563. doi:10.1130/G24628A.1

Clark, C.D., Hughes, A.L.C., Greenwood, S.L., Jordan, C., Sejrup, H.P., 2012. Pattern and timing of retreat of the last British-Irish Ice Sheet. Quat. Sci. Rev. 44, 112–146. doi:10.1016/j.quascirev.2010.07.019

Clark, P.U., Dyke, A.S., Shakun, J.D., Carlson, A.E., Clark, J., Wohlfarth, B., Mitrovica, J.X., Hostetler, S.W., McCabe, a M., 2009. The Last Glacial Maximum. Science 325, 710–714. doi:10.1126/science.1172873

Clark, P.U., Marshall, S.J., Clarke, G.K.C., Hostetler, S.W., Licciardi, J.M., Teller, J.T., 2001. Freshwater forcing of abrupt climate change during the last glaciation. Science 293, 283–287. doi:10.1126/science.1062517

Clarke, G.K.C., 2005. Subglacial processes. Annu. Rev. Earth Planet. Sci. 33, 247–276. doi:10.1146/annurev.earth.33.092203.122621

Clason, C.C., Applegate, P.J., Holmlund, P., 2014. Modelling Late Weichselian evolution of the Eurasian ice sheets forced by surface meltwater-enhanced basal sliding. J. Glaciol. doi:10.3189/2014JoG13J037

Clason, C.C., Greenwood, S.L., Selmes, N., Lea, J.M., Jamieson, S.S.R., Nick, F.M., Holmlund, P., 2016. Controls on the early Holocene collapse of the Bothnian Sea Ice Stream. J. Geophys. Res. Earth Surf. doi:10.1002/2016JF004050

Crémière, A., Lepland, A., Chand, S., Sahy, D., Condon, D.J., Noble, S.R., Martma, T., Thorsnes, T., Sauer, S., Brunstad, H., 2016. Timescales of methane seepage on the Norwegian margin following collapse of the Scandinavian Ice Sheet. Nat. Commun. 7, 11509. doi:10.1038/ncomms11509

Cuzzone, J.K., Clark, P.U., Carlson, A.E., Ullman, D.J., Rinterknecht, V.R., Milne, G.A., Lunkka, J.-P., Wohlfarth, B., Marcott, S.A., Caffee, M., 2016. Final deglaciation of the Scandinavian Ice Sheet and implications for the Holocene global sea-level budget, Earth and Planetary Science Letters. doi:10.1016/j.epsl.2016.05.019

Dahlgren, K.I.T., Vorren, T.O., Stoker, M.S., Nielsen, T., Nygård, A., Sejrup, H.P., 2005. Late Cenozoic

prograding wedges on the NW European continental margin: their formation and relationship to tectonics and climate. Mar. Pet. Geol. 22, 1089–1110. doi:10.1016/j.marpetgeo.2004.12.008

Deschamps, P., Durand, N., Bard, E., Hamelin, B., Camoin, G., Thomas, A.L., Henderson, G.M., Okuno, J., Yokoyama, Y., 2012. Ice-sheet collapse and sea-level rise at the Bølling warming 14,600 years ago. Nature 483, 559–564. doi:10.1038/nature10902

Dunlop, P., Shannon, R., McCabe, M., Quinn, R., Doyle, E., 2010. Marine geophysical evidence for ice sheet extension and recession on the Malin Shelf: New evidence for the western limits of the British Irish Ice Sheet. Mar. Geol. 276, 86–99. doi:10.1016/j.margeo.2010.07.010

Dyke, A.S., Andrews, J.T., Clark, P.U., England, J.H., Miller, G.H., Shaw, J., Veillette, J.J., 2002. The Laurentide and Innuitian ice sheets during the Last Glacial Maximum. Quat. Sci. Rev. 21, 9–31. doi:10.1016/S0277-3791(01)00095-6

Dziewonski, A.M., Anderson, D.L., 1981. Preliminary reference Earth model. Phys. Earth Planet. Inter. 25, 297–356. doi:10.1016/0031-9201(81)90046-7

Ehlers, J., Gibbard, P.L., 2007. The extent and chronology of Cenozoic Global Glaciation. Quat. Int. 164–165, 6–20. doi:10.1016/j.quaint.2006.10.008

Elverhøi, A., Dowdeswell, J.A., Funder, S., Mangerud, J., Stein, R., 1998. Glacial and oceanic history of the polar north atlantic margins: An overview. Quat. Sci. Rev. 17, 1–10. doi:10.1016/S0277-3791(97)00073-5

Epshtein, O.G., Dlugach, A.G., Starovoytov, A. V., Romanyuk, B.F., 2011. Pleistocene sediments of the eastern Barents Sea (Central Deep and Murmansk Bank): Communication 2. Lithological composition and formation conditions. Lithol. Miner. Resour. 46, 220–249. doi:10.1134/S0024490211030047

Evans, D.J.A., Clark, C.D., Mitchell, W.A., 2005. The last British Ice Sheet: A review of the evidence utilised in the compilation of the Glacial Map of Britain. Earth-Science Rev. 70, 253–312. doi:10.1016/j.earscirev.2005.01.001

Evans, D.J.A., Thomson, S.A., 2010. Glacial sediments and landforms of Holderness, eastern England: A glacial depositional model for the North Sea Lobe of the British–Irish Ice Sheet. Earth-Science Rev. 101, 147–189. doi:10.1016/j.earscirev.2010.04.003

Eynaud, F., Zaragosi, S., Scourse, J.D., Mojtahid, M., Bourillet, J.F., Hall, I.R., Penaud, A., Locascio, M., Reijonen, A., 2007. Deglacial laminated facies on the NW European continental margin: The hydrographic significance of British-Irish Ice Sheet deglaciation and Fleuve Manche paleoriver discharges. Geochemistry, Geophys. Geosystems 8, n/a-n/a. doi:10.1029/2006GC001496

Farrell, W.E., Clark, J.A., 1976. On Postglacial Sea Level. Geophys. J. R. Astron. Soc. 46, 647–667. doi:10.1111/j.1365-246X.1976.tb01252.x

Forman, S.L., 1990. Post-glacial relative sea-level history of northwestern Spitsbergen, Svalbard. Geol. Soc. Am. Bull. 102, 1580–1590. doi:10.1130/0016-7606(1990)102<1580:PGRSLH>2.3.CO;2

Forman, S.L., 1989. Late Weichselian glaciation and deglaciation of Forlandsundet area, western Spitsbergen, Svalbard. Boreas 18, 51–60. doi:10.1111/j.1502-3885.1989.tb00370.x

Forman, S.L., Lubinski, D.J., Ingólfsson, Ó., Zeeberg, J.J., Snyder, J.A., Siegert, M.J., Matishov, G.G., 2004. A review of postglacial emergence on Svalbard, Franz Josef Land and Novaya Zemlya, northern Eurasia. Quat. Sci. Rev. 23, 1391–1434. doi:10.1016/j.quascirev.2003.12.007

Forman, S.L., Weihe, R., Lubinski, D., Tarasov, G., Korsun, S., Matishov, G., 1997. Holocene relative

sea-level history of Franz Josef Land, Russia. Geol. Soc. Am. Bull. 109, 1116–1133. doi:10.1130/0016-7606(1997)109

Forsström, P.-L., Greve, R., 2004. Simulation of the Eurasian ice sheet dynamics during the last glaciation. Glob. Planet. Change 42, 59–81. doi:10.1016/j.gloplacha.2003.11.003

Fricker, H.A., Scambos, T., 2009. Connected subglacial lake activity on lower Mercer and Whillans Ice Streams, West Antarctica, 2003–2008. J. Glaciol. 55, 303–315. doi:10.3189/002214309788608813

Fujii, Y., Kusunoki, K., 1982. The role of sublimation and condensation in the formation of ice sheet surface at Mizuho Station, Antarctica. J. Geophys. Res. Ocean. 87, 4293–4300. doi:10.1029/JC087iC06p04293

Gammelsrød, T., Leikvin, Ø., Lien, V., Budgell, W.P., Loeng, H., Maslowski, W., 2009. Mass and heat transports in the NE Barents Sea: Observations and models. J. Mar. Syst. 75, 56–69. doi:10.1016/j.jmarsys.2008.07.010

Gibbard, P.L., 1988. The History of the Great Northwest European Rivers During the Past Three Million Years. Philos. Trans. R. Soc. B Biol. Sci. B318, 559–602. doi:10.1098/rstb.1988.0024

Golledge, N., Hubbard, A., Bradwell, T., 2010. Influence of seasonality on glacier mass balance, and implications for palaeoclimate reconstructions. Clim. Dyn. 35, 757–770. doi:10.1007/s00382-009-0616-6

Golledge, N.R., 2010. Glaciation of Scotland during the Younger Dryas stadial: A review. J. Quat. Sci. 25, 550–566. doi:10.1002/jqs.1319

Golledge, N.R., Hubbard, A., 2005. Evaluating Younger Dryas glacier reconstructions in part of the western Scottish Highlands: A combined empirical and theoretical approach. Boreas 34, 274–286. doi:10.1111/j.1502-3885.2005.tb01101.x

Golledge, N.R., Hubbard, A., Sugden, D.E., 2008. High-resolution numerical simulation of Younger Dryas glaciation in Scotland. Quat. Sci. Rev. 27, 888–904. doi:10.1016/j.quascirev.2008.01.019

Graham, A.G.C., Lonergan, L., Stoker, M.S., 2010. Depositional environments and chronology of Late Weichselian glaciation and deglaciation in the central North Sea. Boreas 39, 471–491. doi:10.1111/j.1502-3885.2010.00144.x

Greenwood, S.L., Clark, C.D., 2009. Reconstructing the last Irish Ice Sheet 2: a geomorphologically-driven model of ice sheet growth, retreat and dynamics. Quat. Sci. Rev. 28, 3101–3123. doi:10.1016/j.quascirev.2009.09.014

Greenwood, S.L., Clason, C.C., Mikko, H., Nyberg, J., Peterson, G., Smith, C.A., 2015. Integrated use of LiDAR and multibeam bathymetry reveals onset of ice streaming in the northern Bothnian Sea. J. Geol. Soc. Sweden 137, 284–292. doi:10.1080/11035897.2015.1055513

Grosswald, M.G., Hughes, T.J., 2002. The Russian component of an Arctic Ice Sheet during the Last Glacial Maximum. Quat. Sci. Rev. 21, 121–146. doi:10.1016/S0277-3791(01)00078-6

Hall, A.M., 2013. The last glaciation of Shetland: Local ice cap or invasive ice sheet? Nor. J. Geol. 93, 229–242.

Hall, A.M., Riding, J.B., Brown, J.F., 2016. The last glaciation in Orkney, Scotland: glacial stratigraphy, event sequence and flow paths. Scottish J. Geol. 52, 90–101. doi:10.1144/sjg2016-002

Hättestrand, C., Clark, C.D., 2006. The glacial geomorphology of Kola Peninsula and adjacent areas in the Murmansk Region, Russia. J. Maps 2, 30–42. doi:10.4113/jom.2006.41

Hijmans, R.J., Cameron, S.E., Parra, J.L., Jones, P.G., Jarvis, A., 2005. Very high resolution interpolated climate surfaces for global land areas. Int. J. Climatol. 25, 1965–1978. doi:10.1002/joc.1276

Hindmarsh, R.C.A., 2004. A numerical comparison of approximations to the Stokes equations used in ice sheet and glacier modeling. J. Geophys. Res. Earth Surf. 109, F01012. doi:10.1029/2003JF000065

Hindmarsh, R.C.A., Stokes, C.R., 2008. Formation mechanisms for ice-stream lateral shear margin moraines. Earth Surf. Process. Landforms 33, 610–626. doi:10.1002/esp.1665

Hoff, U., Rasmussen, T.L., Stein, R., Ezat, M.M., Fahl, K., 2016. Sea ice and millennial-scale climate variability in the Nordic seas 90 kyr ago to present. Nat. Commun. 7:12247. doi:10.1038/ncomms12247

Holmlund, P., Fastook, J., 1993. Numerical modelling provides evidence of a Baltic Ice Stream during the Younger Dryas. Boreas 22, 77–86. doi:10.1111/j.1502-3885.1993.tb00166.x

Hoppe, G., Schytt, V., Häggblom, A., Österholm, H., 1969. Studies of the glacial history of Hopen (Hopen Island), Svalbard. Geogr. Ann. Ser. A, Phys. Geogr. 51, 185–192.

Hormes, A., Gjermundsen, E.F., Rasmussen, T.L., 2013. From mountain top to the deep sea – Deglaciation in 4D of the northwestern Barents Sea ice sheet. Quat. Sci. Rev. 75, 78–99. doi:10.1016/j.quascirev.2013.04.009

Hovland, M., Svensen, H., Forsberg, C.F., Johansen, H., Fichler, C., Fosså, J.H., Jonsson, R., Rueslåtten, H., 2005. Complex pockmarks with carbonate-ridges off mid-Norway: Products of sediment degassing. Mar. Geol. 218, 191–206. doi:10.1016/j.margeo.2005.04.005

Hubbard, A., 2006. The validation and sensitivity of a model of the Icelandic ice sheet. Quat. Sci. Rev. 25, 2297–2313. doi:10.1016/j.quascirev.2006.04.005

Hubbard, A., 2000. The verification and significance of three approaches to longitudinal stresses in high-resolution models of glacier flow. Geogr. Ann. Ser. A, Phys. Geogr. 82, 471–487. doi:10.1111/j.0435-3676.2000.00135.x

Hubbard, A., 1999. High-resolution modeling of the advance of the Younger Dryas ice sheet and its climate in Scotland. Quat. Res. 52, 27–43. doi:10.1006/qres.1999.2055

Hubbard, A., Bradwell, T., Golledge, N., Hall, A., Patton, H., Sugden, D., Cooper, R., Stoker, M., 2009. Dynamic cycles, ice streams and their impact on the extent, chronology and deglaciation of the British–Irish ice sheet. Quat. Sci. Rev. 28, 758–776. doi:10.1016/j.quascirev.2008.12.026

Hubbard, B., Hubbard, A., 1998. Bedrock surface roughness and the distribution of subglacially precipitated carbonate deposits: implications for formation at Glacier de Tsanfleuron, Switzerland. Earth Surf. Process. Landforms 23, 261–270. doi:10.1002/(SICI)1096-9837(199803)23:3<261::AID-ESP848>3.0.CO;2-5

Hughes, A.L.C., Clark, C.D., Jordan, C.J., 2014. Flow-pattern evolution of the last British Ice Sheet. Quat. Sci. Rev. 89, 148–168. doi:10.1016/j.quascirev.2014.02.002

Hughes, A.L.C., Greenwood, S.L., Clark, C.D., 2011. Dating constraints on the last British-Irish Ice Sheet: a map and database. J. Maps 7, 156–184. doi:10.4113/jom.2011.1145

Hughes, A.L.C., Gyllencreutz, R., Lohne, Ø.S., Mangerud, J., Svendsen, J.I., 2016. The last Eurasian ice sheets – a chronological database and time-slice reconstruction, DATED-1. Boreas 45, 1–45. doi:10.1111/bor.12142

Ingólfsson, Ó., Landvik, J.Y., 2013. The Svalbard–Barents Sea ice-sheet – Historical, current and

future perspectives. Quat. Sci. Rev. 64, 33–60. doi:10.1016/j.quascirev.2012.11.034

Jakobsson, M., Björck, S., Alm, G., Andrén, T., Lindeberg, G., Svensson, N.-O., 2007. Reconstructing the Younger Dryas ice dammed lake in the Baltic Basin: Bathymetry, area and volume. Glob. Planet. Change 57, 355–370. doi:10.1016/j.gloplacha.2007.01.006

Jessen, S.P., Rasmussen, T.L., Nielsen, T., Solheim, A., 2010. A new Late Weichselian and Holocene marine chronology for the western Svalbard slope 30,000–0 cal years BP. Quat. Sci. Rev. 29, 1301–1312. doi:10.1016/j.quascirev.2010.02.020

Kageyama, M., Braconnot, P., Harrison, S.P., Haywood, A.M., Jungclaus, J., Otto-Bliesner, B.L., Peterschmitt, J.-Y., Abe-Ouchi, A., Albani, S., Bartlein, P.J., Brierley, C., Crucifix, M., Dolan, A., Fernandez-Donado, L., Fischer, H., Hopcroft, P.O., Ivanovic, R.F., Lambert, F., Lunt, D.J., Mahowald, N.M., Peltier, W.R., Phipps, S.J., Roche, D.M., Schmidt, G.A., Tarasov, L., Valdes, P.J., Zhang, Q., Zhou, T., 2016. PMIP4-CMIP6: the contribution of the Paleoclimate Modelling Intercomparison Project to CMIP6. Geosci. Model Dev. Discuss. 1–46. doi:10.5194/gmd-2016-106

Kameda, T., Azuma, N., Furukawa, T., Ageta, Y., Takahashi, S., 1997. Surface mass balance, sublimation and snow temperatures at Dome Fuji Station, Antarctica, in 1995. Proc. NIPR Symp. Polar Meteorol. Glaciol. 11, 24–34.

Kaufmann, G., Wolf, D., 1996. Deglacial land emergence and lateral upper-mantle heterogeneity in the Svalbard Archipelago-II. Extended results for high-resolution load models. Geophys. J. Int. 127, 125–140. doi:10.1111/j.1365-246X.1996.tb01539.x

Kendall, R.A., Mitrovica, J.X., Milne, G.A., 2005. On post-glacial sea level - II. Numerical formulation and comparative results on spherically symmetric models. Geophys. J. Int. 161, 679–706. doi:10.1111/j.1365-246X.2005.02553.x

Kim, B.-H., Lee, C.-K., Seo, K.-W., Lee, W.S., Scambos, T., 2016. Active subglacial lakes and channelized water flow beneath the Kamb Ice Stream. Cryosph. 10, 2971–2980. doi:10.5194/tc-10-2971-2016

King, E.., Haflidason, H., Sejrup, H.., Løvlie, R., 1998. Glacigenic debris flows on the North Sea Trough Mouth Fan during ice stream maxima. Mar. Geol. 152, 217–246. doi:10.1016/S0025-3227(98)00072-3

Kleman, J., Glasser, N.F., 2007. The subglacial thermal organisation (STO) of ice sheets. Quat. Sci. Rev. 26, 585–597. doi:10.1016/j.quascirev.2006.12.010

Kleman, J., Hättestrand, C., Borgström, I., Stroeven, A., 1997. Fennoscandian palaeoglaciology reconstructed using a glacial geological inversion model. J. Glaciol. 43, 283–299. doi:10.3198/1997JoG43-144-283-299

Klitzke, P., Faleide, J.I., Scheck-Wenderoth, M., Sippel, J., 2015. A lithosphere-scale structural model of the Barents Sea and Kara Sea region. Solid Earth 6, 153–172. doi:10.5194/se-6-153-2015

Koç, N., Klitgaard-Kristensen, D., Hasle, K., Forsberg, C.F., Solheim, A., 2002. Late glacial palaeoceanography of Hinlopen Strait, northern Svalbard. Polar Res. 21, 307–314. doi:10.1111/j.1751-8369.2002.tb00085.x

Kristensen, D.K., Rasmussen, T.L., Koç, N., 2013. Palaeoceanographic changes in the northern Barents Sea during the last 16 000 years - new constraints on the last deglaciation of the Svalbard-Barents Sea Ice Sheet. Boreas 42, 798–813. doi:10.1111/j.1502-3885.2012.00307.x

Kristensen, T.B., Huuse, M., Piotrowski, J. a, Clausen, O.R., 2007. A morphometric analysis of tunnel

valleys in the eastern North Sea based on 3D seismic data. J. Quat. Sci. 22, 801–815. doi:10.1002/jqs.1123

Kroon, D., Austin, W.E.N., Chapman, M.R., Ganssen, G.M., 1997. Deglacial surface circulation changes in the northeastern Atlantic: Temperature and salinity records off NW Scotland on a century scale. Paleoceanography 12, 755–763. doi:10.1029/97PA02289

Lambeck, K., Purcell, A., Zhao, J., Svensson, N.-O., 2010. The Scandinavian Ice Sheet: from MIS 4 to the end of the Last Glacial Maximum. Boreas 39, 410–435. doi:10.1111/j.1502-3885.2010.00140.x

Lambeck, K., Smither, C., Johnston, P., 1998. Sea-level change, glacial rebound and mantle viscosity fornorthern Europe. Geophys. J. Int. 134, 102–144. doi:10.1046/j.1365-246x.1998.00541.x

Landvik, J.Y., Ingólfsson, Ó., Mienert, J., Lehman, S.J., Solheim, A., Elverhøi, A., Ottesen, D., 2005. Rethinking Late Weichselian ice-sheet dynamics in coastal NW Svalbard. Boreas 34, 7–24. doi:10.1111/j.1502-3885.2005.tb01001.x

Larsen, E., Fredin, O., Lyså, A., Amantov, A., Fjeldskaar, W., Ottesen, D., 2016. Causes of time-transgressive glacial maxima positions of the last Scandinavian Ice Sheet. Nor. J. Geol. 96, 159–170. doi:10.17850/njg96-2-06

Larsen, E., Funder, S., Thiede, J., 1999a. Late Quaternary history of northern Russia and adjacent shelves - a synopsis. Boreas 28, 6–11. doi:10.1111/j.1502-3885.1999.tb00203.x

Larsen, E., Kjær, K., Demidov, I., Funder, S., Grøsfjeld, K., Houmark-Nielsen, M., Jensen, M., Linge, H., Lyså, A., 2006. Late Pleistocene glacial and lake history of northwestern Russia. Boreas 35, 394–424. doi:10.1080/03009480600781958

Larsen, E., Lyså, A., Demidov, I., Funder, S., Houmark-Nielsen, M., Kjær, K.H., Murray, A.S., 1999b. Age and extent of the Scandinavian ice sheet in northwest Russia. Boreas 28, 115–132. doi:10.1111/j.1502-3885.1999.tb00209.x

Larsen, N.K., Linge, H., Håkansson, L., Fabel, D., 2012. Investigating the last deglaciation of the Scandinavian Ice Sheet in southwest Sweden with 10Be exposure dating. J. Quat. Sci. 27, 211–220. doi:10.1002/jqs.1536

Laumann, T., Reeh, N., 1993. Sensitivity to climate-change of the mass-balance of glaciers in southern Norway. J. Glaciol. 39, 656–665. doi:10.3198/1993JoG39-133-656-665

Le Meur, E., Huybrechts, P., 1996. A comparison of different ways of dealing with isostasy: examples from modeling the Antarctic ice sheet during the last glacial cycle. Ann. Glaciol. 23, 309–317. doi:10.3198/1996AoG23-309-317

Lericolais, G., Auffret, J.-P., Bourillet, J.-F., 2003. The Quaternary Channel River: seismic stratigraphy of its palaeo-valleys and deeps. J. Quat. Sci. 18, 245–260. doi:10.1002/jqs.759

Li, Y., Napieralski, J., Harbor, J., Hubbard, A., 2007. Identifying patterns of correspondence between modeled flow directions and field evidence: An automated flow direction analysis. Comput. Geosci. 33, 141–150. doi:10.1016/j.cageo.2006.06.016

Lindbäck, K., Pettersson, R., Hubbard, A.L., Doyle, S.H., van As, D., Mikkelsen, A.B., Fitzpatrick, A.A., 2015. Subglacial water drainage, storage, and piracy beneath the Greenland ice sheet. Geophys. Res. Lett. 42, 7606–7614. doi:10.1002/2015GL065393

Linge, H., Olsen, L., Brook, E., Darter, J., 2007. Cosmogenic nuclide surface exposure ages from Nordland, northern Norway: implications for deglaciation in a coast to inland transect. Nor. J. Geol. 87, 269–280.

Livingstone, S.J., Clark, C.D., Piotrowski, J.A., Tranter, M., Bentley, M.J., Hodson, A., Swift, D.A., Woodward, J., 2012. Theoretical framework and diagnostic criteria for the identification of palaeo-subglacial lakes. Quat. Sci. Rev. 53, 88–110. doi:10.1016/j.quascirev.2012.08.010

Livingstone, S.J., Clark, C.D., Tarasov, L., 2013a. Modelling North American palaeo-subglacial lakes and their meltwater drainage pathways. Earth Planet. Sci. Lett. 375, 13–33. doi:10.1016/j.epsl.2013.04.017

Livingstone, S.J., Clark, C.D., Woodward, J., Kingslake, J., 2013b. Potential subglacial lake locations and meltwater drainage pathways beneath the Antarctic and Greenland ice sheets. Cryosph. 7, 1721–1740. doi:10.5194/tc-7-1721-2013

Livingstone, S.J., Piotrowski, J.A., Bateman, M.D., Ely, J.C., Clark, C.D., 2015. Discriminating between subglacial and proglacial lake sediments: an example from the Dänischer Wohld Peninsula, northern Germany. Quat. Sci. Rev. 112, 86–108. doi:10.1016/j.quascirev.2015.01.030

Lubinski, D.J., Forman, S.L., Miller, G.H., 1999. Holocene glacier and climate fluctuations on Franz Josef Land, Arctic Russia, 80°N. Quat. Sci. Rev. 18, 85–108. doi:10.1016/S0277-3791(97)00105-4

Lubinski, D.J., Polyak, L., Forman, S.L., 2001. Freshwater and Atlantic Water inflows to the deep northern Barents and Kara seas since ca 13 14C ka: Foraminifera and stable isotopes. Quat. Sci. Rev. 20, 1851–1879. doi:10.1016/S0277-3791(01)00016-6

Luckman, A., Benn, D.I., Cottier, F., Bevan, S., Nilsen, F., Inall, M., 2015. Calving rates at tidewater glaciers vary strongly with ocean temperature. Nat. Commun. 6, 8566. doi:10.1038/ncomms9566

Lundqvist, J., 2007. Surging ice and break-down of an ice dome – a deglaciation model for the Gulf of Bothnia. GFF 129, 329–336. doi:10.1080/11035890701294329

Lundqvist, J., 1990. The Younger Dryas event in Scandinavia, in: Lundqvist, J., Saarnisto, M. (Eds.), Termination of the Pleistocene. Geological Survey of Finland, pp. 5–24.

Lundqvist, J., Saarnisto, M., 1995. Summary of project IGCP-253. Quat. Int. 28, 9–18. doi:10.1016/1040-6182(95)00046-L

Lundqvist, J., Wohlfarth, B., 2000. Timing and east–west correlation of south Swedish ice marginal lines during the Late Weichselian. Quat. Sci. Rev. 20, 1127–1148. doi:10.1016/S0277-3791(00)00142-6

Lunkka, J.-P., Putkinen, N., Miettinen, A., 2012. Shoreline displacement in the Belomorsk area, NW Russia during the Younger Dryas Stadial. Quat. Sci. Rev. 37, 26–37. doi:10.1016/j.quascirev.2012.01.023

Mangerud, J., 2004. Ice sheet limits in Norway and on the Norwegian continental shelf, in: Ehlers, J., Gibbard, P.L. (Eds.), Developments in Quaternary Sciences. Quaternary Glaciations Extent and Chronology Part I: Europe. Elsevier B.V., pp. 271–294. doi:10.1016/S1571-0866(04)80078-2

Mangerud, J., Landvik, J.Y., 2007. Younger Dryas cirque glaciers in western Spitsbergen: smaller than during the Little Ice Age. Boreas 36, 278–285. doi:10.1111/j.1502-3885.2007.tb01250.x

Mangerud, J., Svendsen, J.I., 1990. Deglaciation chronology inferred from marine sediments in a proglacial lake basin, western Spitsbergen, Svalbard. Boreas 19, 249–272. doi:10.1111/j.1502-3885.1990.tb00450.x

Marshall, S.J., Björnsson, H., Flowers, G.E., Clarke, G.K.C., 2005. Simulation of Vatnajökull ice cap dynamics. J. Geophys. Res. Earth Surf. 110, F03009. doi:10.1029/2004JF000262

McCabe, A.M., Ó Cofaigh, C., 1994. Sedimentation in a subglacial lake, Enniskerry, eastern Ireland. Sediment. Geol. 91, 57–95. doi:10.1016/0037-0738(94)90123-6

Ménot, G., Bard, E., Rostek, F., Weijers, J.W.H., Hopmans, E.C., Schouten, S., Sinninghe Damsté, J.S., 2006. Early reactivation of European rivers during the last deglaciation. Science 313, 1623–1625. doi:10.1126/science.1130511

Mitrovica, J.X., Milne, G.A., 2003. On post-glacial sea level: I. General theory. Geophys. J. Int. 154, 253–267. doi:10.1046/j.1365-246X.2003.01942.x

Müller, J., Stein, R., 2014. High-resolution record of late glacial and deglacial sea ice changes in Fram Strait corroborates ice–ocean interactions during abrupt climate shifts. Earth Planet. Sci. Lett. 403, 446–455. doi:10.1016/j.epsl.2014.07.016

Munro-Stasiuk, M.J., 2003. Subglacial Lake McGregor, south-central Alberta, Canada. Sediment. Geol. 160, 325–350. doi:10.1016/S0037-0738(03)00090-3

Napieralski, J., Hubbard, A., Li, Y., Harbor, J., Stroeven, A.P., Kleman, J., Alm, G., Jansson, K.N., 2007. Towards a GIS assessment of numerical ice-sheet model performance using geomorphological data. J. Glaciol. 53, 71–83. doi:10.3189/172756507781833884

Näslund, J.-O., Jansson, P., Fastook, J.L., Johnson, J., Andersson, L., 2005. Detailed spatially distributed geothermal heat-flow data for modeling of basal temperatures and meltwater production beneath the Fennoscandian ice sheet. Ann. Glaciol. 40, 95–101. doi:10.3189/172756405781813582

Nesje, A., Dahl, S.O., Bakke, J., 2004. Were abrupt Lateglacial and early-Holocene climatic changes in northwest Europe linked to freshwater outbursts to the North Atlantic and Arctic Oceans? The Holocene 14, 299–310. doi:10.1191/0959683604hl708fa

O'Regan, M., Greenwood, S.L., Preto, P., Swärd, H., Jakobsson, M., 2016. Geotechnical and sedimentary evidence for thick-grounded ice in southern Lake Vättern during deglaciation. GFF 138, 355–366. doi:10.1080/11035897.2015.1055511

Ojala, A.E.K., 2016. Appearance of De Geer moraines in southern and western Finland — Implications for reconstructing glacier retreat dynamics. Geomorphology 255, 16–25. doi:10.1016/j.geomorph.2015.12.005

Ottesen, D., Dowdeswell, J.A., Rise, L., 2005. Submarine landforms and the reconstruction of fast-flowing ice streams within a large Quaternary ice sheet: The 2500-km-long Norwegian-Svalbard margin (57°–80°N). Geol. Soc. Am. Bull. 117, 1033. doi:10.1130/B25577.1

Ottesen, D., Stokes, C.R., Bøe, R., Rise, L., Longva, O., Thorsnes, T., Olesen, O., Bugge, T., Lepland, A., Hestvik, O.B., 2016. Landform assemblages and sedimentary processes along the Norwegian Channel Ice Stream. Sediment. Geol. 338, 115–137. doi:10.1016/j.sedgeo.2016.01.024

Patton, H., Andreassen, K., Bjarnadóttir, L.R., Dowdeswell, J.A., Winsborrow, M.C.M., Noormets, R., Polyak, L., Auriac, A., Hubbard, A., 2015. Geophysical constraints on the dynamics and retreat of the Barents Sea Ice Sheet as a palaeo-benchmark for models of marine ice-sheet deglaciation. Rev. Geophys. 53, 1051–1098. doi:10.1002/2015RG000495

Patton, H., Hubbard, A., Andreassen, K., Winsborrow, M., Stroeven, A.P., 2016. The build-up, configuration, and dynamical sensitivity of the Eurasian ice-sheet complex to Late Weichselian climatic and oceanic forcing. Quat. Sci. Rev. 153, 97–121. doi:10.1016/j.quascirev.2016.10.009

Patton, H., Hubbard, A., Glasser, N.F., Bradwell, T., Golledge, N.R., 2013a. The last Welsh Ice Cap: Part 1 - Modelling its evolution, sensitivity and associated climate. Boreas 42, 471–490.

doi:10.1111/j.1502-3885.2012.00300.x

Patton, H., Hubbard, A.L., Bradwell, T., Glasser, N.F., Hambrey, M.J., Clark, C.D., 2013b. Rapid marine deglaciation: asynchronous retreat dynamics between the Irish Sea Ice Stream and terrestrial outlet glaciers. Earth Surf. Dyn. 1, 53–65. doi:10.5194/esurf-1-53-2013

Peltier, W.R., 2004. Global glacial isostasy and the surface of the ice-age Earth: The ICE-5G (VM2) Model and GRACE. Annu. Rev. Earth Planet. Sci. 32, 111–149. doi:10.1146/annurev.earth.32.082503.144359

Peltier, W.R., Argus, D.F., Drummond, R., 2015. Space geodesy constrains ice age terminal deglaciation: The global ICE-6G_C (VM5a) model. J. Geophys. Res. Solid Earth 120, 450–487. doi:10.1002/2014JB011176

Peters, J.L., Benetti, S., Dunlop, P., Ó Cofaigh, C., 2015. Maximum extent and dynamic behaviour of the last British–Irish Ice Sheet west of Ireland. Quat. Sci. Rev. 128, 48–68. doi:10.1016/j.quascirev.2015.09.015

Pollard, D., DeConto, R.M., 2007. A coupled ice-sheet/ice-shelf/sediment model applied to a marine-margin flowline: forced and unforced variations., in: Hambrey, M.J., Christoffersen, P., Glasser, N.F., Hubbard, B. (Eds.), Glacial Sedimentary Processes and Products. Blackwell Publishing Ltd, Oxford.

Polyak, L., Lehman, S.J., Gataullin, V., Timothy Jull, A.J., 1995. Two-step deglaciation of the southeastern Barents Sea. Geology 23, 567–571. doi:10.1130/0091-7613(1995)023

Portnov, A., Vadakkepuliyambatta, S., Mienert, J., Hubbard, A., 2016. Ice-sheet-driven methane storage and release in the Arctic. Nat. Commun. 7, 10314. doi:10.1038/ncomms10314

Praeg, D., McCarron, S., Dove, D., Ó Cofaigh, C., Scott, G., Monteys, X., Facchin, L., Romeo, R., Coxon, P., 2015. Ice sheet extension to the Celtic Sea shelf edge at the Last Glacial Maximum. Quat. Sci. Rev. 111, 107–112. doi:10.1016/j.quascirev.2014.12.010

Rasmussen, T.L., Thomsen, E., Ślubowska, M.A., Jessen, S., Solheim, A., Koç, N., 2007. Paleoceanographic evolution of the SW Svalbard margin (76°N) since 20,000 14C yr BP. Quat. Res. 67, 100–114. doi:10.1016/j.yqres.2006.07.002

Renssen, H., Isarin, R.F.B., Jacob, D., Podzun, R., Vandenberghe, J., 2001. Simulation of the Younger Dryas climate in Europe using a regional climate model nested in an AGCM: preliminary results. Glob. Planet. Change 30, 41–57. doi:10.1016/S0921-8181(01)00076-5

Reusche, M., Winsor, K., Carlson, A.E., Marcott, S.A., Rood, D.H., Novak, A., Roof, S., Retelle, M., Werner, A., Caffee, M., Clark, P.U., 2014. 10Be surface exposure ages on the late-Pleistocene and Holocene history of Linnébreen on Svalbard. Quat. Sci. Rev. 89, 5–12. doi:10.1016/j.quascirev.2014.01.017

Rinterknecht, V.R., Clark, P.U., Raisbeck, G.M., Yiou, F., Bitinas, A., Brook, E.J., Marks, L., Zelčs, V., Lunkka, J.-P., Pavlovskaya, I.E., Piotrowski, J.A., Raukas, A., 2006. The last deglaciation of the southeastern sector of the Scandinavian ice sheet. Science 311, 1449–1452. doi:10.1126/science.1120702

Rise, L., Bellec, V.K., Chand, S., Bøe, R., 2015. Pockmarks in the southwestern Barents Sea and-Finnmark fjords. Nor. J. Geol. 94, 263–282.

Ritzmann, O., Faleide, J.I., 2009. The crust and mantle lithosphere in the Barents Sea/Kara Sea region. Tectonophysics 470, 89–104. doi:10.1016/j.tecto.2008.06.018

Rüther, D.C., Mattingsdal, R., Andreassen, K., Forwick, M., Husum, K., 2011. Seismic architecture and

sedimentology of a major grounding zone system deposited by the Bjørnøyrenna Ice Stream during Late Weichselian deglaciation. Quat. Sci. Rev. 30, 2776–2792. doi:10.1016/j.quascirev.2011.06.011

Salvigsen, O., 1981. Radiocarbon dated raised beaches in Kong Karls Land, Svalbard, and their consequences for the glacial history of the Barents Sea area. Geogr. Ann. Ser. A, Phys. Geogr. 63, 283. doi:10.2307/520841

Schoof, C., 2007. Marine ice-sheet dynamics. Part 1. The case of rapid sliding. J. Fluid Mech. 573, 27. doi:10.1017/S0022112006003570

Scourse, J.D., Haapaniemi, A.I., Colmenero-Hidalgo, E., Peck, V.L., Hall, I.R., Austin, W.E.N., Knutz, P.C., Zahn, R., 2009. Growth, dynamics and deglaciation of the last British–Irish ice sheet: the deep-sea ice-rafted detritus record. Quat. Sci. Rev. 28, 3066–3084. doi:10.1016/j.quascirev.2009.08.009

Sejrup, H.P., Clark, C.D., Hjelstuen, B.O., 2016. Rapid ice sheet retreat triggered by ice stream debuttressing: Evidence from the North Sea. Geology 44, 355–358. doi:10.1130/G37652.1

Sejrup, H.P., Hjelstuen, B.O., Nygård, A., Haflidason, H., Mardal, I., 2015. Late Devensian ice-marginal features in the central North Sea - processes and chronology. Boreas 44, 1–13. doi:10.1111/bor.12090

Serebryanny, L., Andreev, A., Malyasova, E., Tarasov, P., Romanenko, F., 1998. Lateglacial and early-Holocene environments of Novaya Zemlya and the Kara Sea Region of the Russian Arctic. The Holocene 8, 323–330. doi:10.1191/095968398677085532

Serov, P., Vadakkepuliyambatta, S., Mienert, J., Patton, H., Portnov, A., Silyakova, A., Panieri, G., Carroll, M., Carroll, J., Andreassen, K., Hubbard, A., n.d. The post-glacial response of Arctic Ocean gas hydrates to climatic amelioration. Proc. Natl. Acad. Sci.

Shreve, R.L., 1972. Movement of water in glaciers. J. Glaciol. 11, 205–214. doi:10.1017/S002214300002219X

Siegert, M.J., Dowdeswell, J.A., 2004. Numerical reconstructions of the Eurasian Ice Sheet and climate during the Late Weichselian. Quat. Sci. Rev. 23, 1273–1283. doi:10.1016/j.quascirev.2003.12.010

Ślubowska-Woldengen, M., Rasmussen, T.L., Koç, N., Klitgaard-Kristensen, D., Nilsen, F., Solheim, A., 2007. Advection of Atlantic Water to the western and northern Svalbard shelf since 17,500calyr BP. Quat. Sci. Rev. 26, 463–478. doi:10.1016/j.quascirev.2006.09.009

Small, D., Clark, C.D., Chiverrell, R.C., Smedley, R.K., Bateman, M.D., Duller, G.A.T., Ely, J.C., Fabel, D., Medialdea, A., Moreton, S.G., 2017. Devising quality assurance procedures for assessment of legacy geochronological data relating to deglaciation of the last British-Irish Ice Sheet. Earth-Science Rev. 164, 232–250. doi:10.1016/j.earscirev.2016.11.007

Small, D., Fabel, D., 2016. Was Scotland deglaciated during the Younger Dryas? Quat. Sci. Rev. 145, 259–263. doi:10.1016/j.quascirev.2016.05.031

Squeak, P.P., Diddlesworth, I.R., 1987. The influence of ptarmigan population dynamics on the thermal regime of the Laurentide Ice Sheet : the surface boundary condition. IAHS Publ.

Steffen, H., Kaufmann, G., 2005. Glacial isostatic adjustment of Scandinavia and northwestern Europe and the radial viscosity structure of the Earth's mantle. Geophys. J. Int. 163, 801–812. doi:10.1111/j.1365-246X.2005.02740.x

Stokes, C.R., Clark, C.D., 2001. Palaeo-ice streams. Quat. Sci. Rev. 20, 1437–1457.

doi:10.1016/S0277-3791(01)00003-8

Stokes, C.R., Tarasov, L., Blomdin, R., Cronin, T.M., Fisher, T.G., Gyllencreutz, R., Hättestrand, C., Heyman, J., Hindmarsh, R.C.A., Hughes, A.L.C., Jakobsson, M., Kirchner, N., Livingstone, S.J., Margold, M., Murton, J.B., Noormets, R., Peltier, W.R., Peteet, D.M., Piper, D.J.W., Preusser, F., Renssen, H., Roberts, D.H., Roche, D.M., Saint-Ange, F., Stroeven, A.P., Teller, J.T., 2015. On the reconstruction of palaeo-ice sheets: Recent advances and future challenges. Quat. Sci. Rev. 125, 15–49. doi:10.1016/j.quascirev.2015.07.016

Stroeven, A.P., Fabel, D., Harbor, J.M., Fink, D., Caffee, M.W., Dahlgren, T., 2011. Importance of sampling across an assemblage of glacial landforms for interpreting cosmogenic ages of deglaciation. Quat. Res. 76, 148–156. doi:10.1016/j.yqres.2011.04.004

Stroeven, A.P., Hättestrand, C., Kleman, J., Heyman, J., Fabel, D., Fredin, O., Goodfellow, B.W., Harbor, J.M., Jansen, J.D., Olsen, L., Caffee, M.W., Fink, D., Lundqvist, J., Rosqvist, G.C., Strömberg, B., Jansson, K.N., 2016. Deglaciation of Fennoscandia. Quat. Sci. Rev. 147, 91–121. doi:10.1016/j.quascirev.2015.09.016

Stroeven, A.P., Heyman, J., Fabel, D., Björck, S., Caffee, M.W., Fredin, O., Harbor, J.M., 2015. A new Scandinavian reference 10Be production rate. Quat. Geochronol. 29, 104–115. doi:10.1016/j.quageo.2015.06.011

Strömberg, B., 1985. Revision of the lateglacial Swedish varve chronology. Boreas 14, 101–105. doi:10.1111/j.1502-3885.1985.tb00896.x

Sugden, D., John, B.S., 1976. Glaciers and Landscape. Arnold, London.

Sutinen, R., Jakonen, M., Liwata, P., Hyvönen, E., 2007. Late Weichselian sheetflow drainage of subglacial Lokka ice lake. Geol. Surv. Finl. Spec. Pap. 46, 55–62.

Svendsen, J.I., Alexanderson, H., Astakhov, V.I., Demidov, I., Dowdeswell, J.A., Funder, S., Gataullin, V., Henriksen, M., Hjort, C., Houmark-Nielsen, M., Hubberten, H.W., Ingólfsson, Ó., Jakobsson, M., Kjær, K.H., Larsen, E., Lokrantz, H., Lunkka, J.P., Lysså, A., Mangerud, J., Matiouchkov, A., Murray, A., Möller, P., Niessen, F., Nikolskaya, O., Polyak, L., Saarnisto, M., Siegert, C., Siegert, M.J., Spielhagen, R.F., Stein, R., 2004. Late Quaternary ice sheet history of northern Eurasia. Quat. Sci. Rev. 23, 1229–1271. doi:10.1016/j.quascirev.2003.12.008

Svendsen, J.I., Briner, J.P., Mangerud, J., Young, N.E., 2015. Early break-up of the Norwegian Channel Ice Stream during the Last Glacial Maximum. Quat. Sci. Rev. 107, 231–242. doi:10.1016/j.quascirev.2014.11.001

Teichert, B.M.A., Eisenhauer, A., Bohrmann, G., Haase-Schramm, A., Bock, B., Linke, P., 2003. U/Th systematics and ages of authigenic carbonates from Hydrate Ridge, Cascadia Margin: recorders of fluid flow variations. Geochim. Cosmochim. Acta 67, 3845–3857. doi:10.1016/S0016-7037(03)00128-5

Toucanne, S., Soulet, G., Freslon, N., Silva Jacinto, R., Dennielou, B., Zaragosi, S., Eynaud, F., Bourillet, J.-F., Bayon, G., 2015. Millennial-scale fluctuations of the European Ice Sheet at the end of the last glacial, and their potential impact on global climate. Quat. Sci. Rev. 123, 113–133. doi:10.1016/j.quascirev.2015.06.010

Toucanne, S., Zaragosi, S., Bourillet, J.F., Cremer, M., Eynaud, F., Van Vliet-Lanoë, B., Penaud, A., Fontanier, C., Turon, J.L., Cortijo, E., Gibbard, P.L., 2009. Timing of massive “Fleuve Manche” discharges over the last 350kyr: insights into the European ice-sheet oscillations and the European drainage network from MIS 10 to 2. Quat. Sci. Rev. 28, 1238–1256. doi:10.1016/j.quascirev.2009.01.006

van den Berg, J., van de Wal, R., Oerlemans, H., 2008a. A mass balance model for the Eurasian Ice Sheet for the last 120,000 years. Glob. Planet. Change 61, 194–208. doi:10.1016/j.gloplacha.2007.08.015

van den Berg, J., van de Wal, R.S.W., Milne, G.A., Oerlemans, J., 2008b. Effect of isostasy on dynamical ice sheet modeling: A case study for Eurasia. J. Geophys. Res. 113, B05412. doi:10.1029/2007JB004994

van der Veen, C.J., 1999. Fundamentals of glacier dynamics. A.A. Balkema, Rotterdam.

Waelbroeck, C., Labeyrie, L., Michel, E., Duplessy, J.C., McManus, J.F., Lambeck, K., Balbon, E., Labracherie, M., 2002. Sea-level and deep water temperature changes derived from benthic foraminifera isotopic records. Quat. Sci. Rev. 21, 295–305. doi:10.1016/S0277-3791(01)00101-9

Walker, D.P., Brandon, M.A., Jenkins, A., Allen, J.T., Dowdeswell, J.A., Evans, J., 2007. Oceanic heat transport onto the Amundsen Sea shelf through a submarine glacial trough. Geophys. Res. Lett. 34, L02602. doi:10.1029/2006GL028154

Winsborrow, M.C.M., Andreassen, K., Corner, G.D., Laberg, J.S., 2010. Deglaciation of a marine-based ice sheet: Late Weichselian palaeo-ice dynamics and retreat in the southern Barents Sea reconstructed from onshore and offshore glacial geomorphology. Quat. Sci. Rev. 29, 424–442. doi:10.1016/j.quascirev.2009.10.001

Wright, A., Siegert, M., 2012. A fourth inventory of Antarctic subglacial lakes. Antarct. Sci. 24, 659–664. doi:10.1017/S095410201200048X